



# On the layerwise finite element formulation for static and free vibration analysis of functionally graded sandwich plates

Hicham Hirane<sup>1</sup> · Mohamed-Ouejdi Belarbi<sup>1</sup> · Mohammed Sid Ahmed Houari<sup>2</sup> · Abdelouahed Tounsi<sup>3,4,5</sup>

Received: 20 June 2020 / Accepted: 17 December 2020 / Published online: 24 January 2021  
© The Author(s), under exclusive licence to Springer-Verlag London Ltd. part of Springer Nature 2021

## Abstract

This paper presents a novel  $C^0$  higher-order layerwise finite element model for static and free vibration analysis of functionally graded materials (FGM) sandwich plates. The proposed layerwise model, which is developed for multilayer composite plates, supposes higher-order displacement field for the core and first-order displacement field for the face sheets maintaining a continuity of displacement at layer. Unlike the conventional layerwise models, the present one has an important feature that the number of variables is fixed and does not increase when increasing the number of layers. Thus, based on the suggested model, a computationally efficient  $C^0$  eight-node quadrilateral element is developed. Indeed, the new element is free of shear locking phenomenon without requiring any shear correction factors. Three common types of FGM plates, namely, (i) isotropic FGM plates; (ii) sandwich plates with FGM face sheets and homogeneous core and (iii) sandwich plates with homogeneous face sheets and FGM core, are considered in the present work. Material properties are assumed graded in the thickness direction according to a simple power law distribution in terms of the volume power laws of the constituents. The equations of motion of the FGM sandwich plate are obtained via the classical Hamilton's principle. Numerical results of present model are compared with 2D, quasi-3D, and 3D analytical solutions and other predicted by advanced finite element models reported in the literature. The results indicate that the developed finite element model is promising in terms of accuracy and fast rate of convergence for both thin and thick FGM sandwich plates. Finally, it can be concluded that the proposed model is accurate and efficient in predicting the bending and free vibration responses of FGM sandwich plates.

**Keywords** Functionally graded materials · Sandwich plates · Layerwise · Bending analysis · Free vibration · Finite element method

## 1 Introduction

Sandwich structures are one of the most functional forms of advanced composite structures developed by engineers. They have been ubiquitously applied in modern engineering especially in the civil constructions, marine industry, automobile, aerospace applications and other industrial applications due to their excellent mechanical performances, i.e., high bending rigidity and vibration characteristics, high ratio of stiffness to weight, excellent durability. Sandwich constructions consist of two outer strong layers and an inner relatively thick, lightweight core material [1]. Sandwich structure has become even more attractive to the introduction of advanced composite materials for the face sheets like functionally graded ceramic–metal materials [2]. The considerable advantages offered by FGM over conventional composite materials are to eliminates the interface problems and thus the stress distribution becomes smooth [3].

✉ Mohamed-Ouejdi Belarbi  
mo.belarbi@univ-biskra.dz; Belarbi.m.w@gmail.com

<sup>1</sup> Laboratoire de Génie Energétique et Matériaux, LGEM, Université de Biskra, B.P. 145 R.P., 07000 Biskra, Algeria

<sup>2</sup> Laboratoire d'Etude des Structures et de Mécanique des Matériaux, Département de Génie Civil, Faculté des Sciences et de la Technologie, Université Mustapha Stambouli, Mascara, Algérie

<sup>3</sup> YFL (Yonsei Frontier Lab), Yonsei University, Seoul, Korea

<sup>4</sup> Department of Civil and Environmental Engineering, King Fahd University of Petroleum and Minerals, Dhahran 31261, Eastern Province, Saudi Arabia

<sup>5</sup> Material and Hydrology Laboratory, Faculty of Technology, Civil Engineering Department, University of Sidi Bel Abbes, Sidi Bel Abbes, Algeria

Subsequently, a number of studies have been performed to studies the static, vibration, and buckling of functionally graded structures due to the increased relevance of the FGM structural components in the design of engineering structures [4].

For a design purpose, it is necessary to understand the mechanical behavior of FGM sandwich plates. Several computational models, both analytically and numerically, have been proposed by researchers to predict accurately the vibrational characteristics of FGM structures. Anderson [5] presented a three-dimensional (3D) analytical elasticity solution for a sandwich plates with a functionally graded (FG) core subjected to transverse loading using a rigid spherical indenter. Vel and Batra [6] proposed an exact elasticity solution using the power series expansion method to study the free and forced vibrations behaviour of simply supported FGM rectangular plates. The authors used Mori–Tanaka method to estimate the effective material properties. Li, Iu et al. [3] presented a 3D analytical elasticity solutions based on Ritz method, in conjunction with Chebyshev polynomial series, for free vibration analysis of FGM sandwich rectangular plates. They considered two types of FGM sandwich plates with simply supported and clamped boundary conditions. Similarly, Kashtalyan and Menshykova [7] developed a 3D analytical elasticity solutions based on Plevako method for simply supported sandwich plates with a FG core. They concluded from their results that use of functionally graded core eliminates discontinuity of the in-plane normal stress across the face sheet/core interface, and reduces the magnitude of stresses in the face sheets and deflection of panels.

From the review paper of Swaminathan et al. [8], the 3D analytical elasticity solution are becomes difficult and tedious when a power law is used for the gradation of material properties. In addition, boundary value and eigenvalue problems of 3D elasticity equations are hard to solve. Hence, the development of accurate two-dimensional (2D) models has drawn a considerable amount of attention from researchers to represent accurately the behavior of FGM sandwich structures.

In the framework of 2D approaches, Equivalent Single-Layer (ESL) theories of different orders [Classical Plate Theory (CPT), First-order Shear Deformation Theory (FSDT) and Higher order Shear Deformation Theories (HSDT)] have been used. The classical plate theory based on the Kirchhoff's assumptions ignores the transverse shear strain and is suitable only to studies thin plates/shells [9–14]. However, it is not appropriate for the moderately thick and thick plates, which require that the transverse and normal strain should be taken into account. First-order shear deformation theory considers a constant transverse shear deformation effects and gives acceptable results for thick and thin plates [15–19], but needs a shear correction factor which is hard to find as it depends on the geometries, material properties and

boundary conditions of each problem [20]. To overcome the limitation of CLPT and FSDT, various HSDT (sinusoidal, exponential, hyperbolic, inverse-hyperbolic, and third-order shear deformation theory) were developed for a better representation of transverse shear stresses without the use of correction factors [21–30]. These theories include higher-order terms in the approximation of the in-plane displacement fields and satisfy zero shear stress conditions at top and bottom surfaces of plates.

Recently, several 2D analytical models, based on HSDT, have been performed to examine the realistic structural behavior of FGM sandwich plates/shells. Zenkour [23, 31] investigated the static response, buckling and free vibration of a simply supported sandwich plates with FG face sheets and homogeneous core using sinusoidal shear deformation plate theory (SSDPT). Hadji et al. [32] employed a four-variable refined plate theory (RPT) to study the free vibration analysis of FGM sandwich rectangular plates. The closed form solutions are obtained by using the Navier technique. Neves et al. [33–35] investigated the static, free vibration and buckling analyses of FGM isotropic and sandwich plates by using various non-polynomial functions. Ye et al. [36] presented a new higher-order refined model for the static and free vibration analysis of sandwich plate with FGM soft core. Meziane et al. [37] developed an efficient and simple refined shear deformation theory for the vibration and buckling of sandwich plate resting on elastic foundations under various boundary conditions. The core layer is considered as a homogeneous material and the face sheets is assumed as FGM. The researchers used a new exponential law distribution to estimate the material properties of the sandwich plate. Nguyen et al. [38] proposed a new inverse trigonometric shear deformation theory for the static, buckling and free vibration analyses of simply supported FGM isotropic and sandwich plates. In a later study, Bennoun et al. [39] made an attempt to analyze the free vibration behavior of simply supported square FGM sandwich plates using a new five-variable refined plate theory. Recently, Meksi et al. [40] proposed a new four-variable shear deformation plate theory for the bending, buckling and free vibration responses of FGM sandwich plates. Similarly, Sayyad and Ghugal [41] presented a unified five-variable shear deformation theory for the bending analysis of a simply supported softcore and hardcore functionally graded sandwich beams and plates. More recently, a novel displacement field based on exponential-trigonometric HSDT was developed by Belkhodja et al. [42] to study the bending, free vibration, and buckling analysis of FGM plates. The material properties of the plate are estimated as power (P-FGM) and exponential (E-FGM) function. Saini and Lal [43] studied a free vibration analysis of bi-directional functionally graded circular plates subjected to two-dimensional temperature variation using FSDT.

From the previous literature review, we found that the majority of researchers used analytical models to study the behavior of FGM sandwich plates/shells. However, the analytical approaches were limited to simple geometries, certain types of gradation of material properties (e.g., exponential or power law distribution), special loading cases and specific types of boundary conditions [44, 45]. Therefore, the numerical methods have been chosen to analyze the complex behavior of FGM structures. Among them, the finite element method (FEM) is the most popular one. The FEM has several advantages in terms of ease in implementation of complex loading, arbitrary grading properties, varying boundary conditions and ease of solution process [46, 47].

Das et al. [48] developed a  $C^1$  triangular plate element based on HSDT for modelling thick sandwich panels with or without FG core subjected to thermo-mechanical loading. Talha and Singh [49] developed a  $C^0$  continuous nine-node quadrilateral isoparametric plate element with 13 degrees-of-freedom (DOFs) for the bending and vibration analysis of FGM plates using HSDT. With a similar effort, Natarajan and Manickam [50] carried-out the static deflection and free vibration analysis of thick/thin FGM sandwich plates using a  $C^0$  eight nodes quadrilateral element with 13 DOFs per node on the basis of HSDT. Nguyen et al. [51] developed a new  $C^0$  three-node triangular element having 7 DOFs for static and vibration analysis of FGM isotropic and sandwich plates using HSDT. The formulation of this element is based on the Mixed Interpolation of Tensorial Components (MITC) approach. In the same year, a  $C^0$  nine-node quadrilateral plate element based on HSDT is developed by Gupta et al. [52] to determine the natural frequencies of FGM plate with various boundary conditions. The influences of volume fraction indices, geometry, material inhomogeneity and various boundary conditions on the free vibration of FGM plates were demonstrated. In another study, A hybrid-mixed, four-node, quadrilateral element for the 3D stress analysis of FGM plates is developed by Kulikov et al. [53] using the method of sampling surfaces (SaS).

Based on the above discussed literature review, it appears that a considerable number of finite element models, based on ESL theories, were used in the analysis of FGM structures. The main advantages of ESL models are their inherent simplicity and their low computational cost, due to the number of variables is independent of the number of layers. However, ESL approach fails to capture precisely the local behavior of FGM sandwich structures [54, 55]. Therefore, the use of layerwise (LW) theory, in which the DOFs are linked to specific layers, is important for accurate analyses of thin and thick FGM structures [46, 56–63]. The LW theory provides a kinematically correct representation of the strain field in discrete layers [64, 65]. Liu et al. [66] studied the free vibration analysis of FGMs sandwich plates by using a refined higher-order layerwise model with ANSYS

software. The authors adopted a FSDT for the face sheets and a 3D-elasticity solution for the core. The FGM face sheets is modeled using the solid46 element, whereas the homogeneous flexible core is modeled using the solid45 element. Pandey and Pradyumna [46] presented a new high-order layerwise plate formulation for static and free vibration analyses of symmetric FGM sandwich plates. A high order displacement field is used for the middle layer and a first-order displacement field for top and bottom layers. The authors used an eight-node isoparametric element containing 104 DOFs to model the plate. The effective material properties of the FGM are computed using rule of mixture (ROM).

From the best knowledge of authors, the literature on the analysis of free vibration response of FGM sandwich plates using LW finite element formulation is very few. Therefore, combining the advantage of ESL theories, LW theory and finite element formulation, an efficient layerwise  $C^0$  finite element model is presented to investigate the bending and free vibration responses of thick/thin FGM sandwich plates. The presented model is an extension of the authors' earlier model presented in [58]. The face sheets and the core are modeled individually using, respectively, the FSDT and the HSDT. Compatibility conditions are imposed at face sheets/core interfaces to satisfy the interlaminar displacement continuity. Moreover, an eight-node quadrilateral isoparametric element with 13 DOFs per node is developed based on the proposed model. Three common types of functionally graded plates are studied: (i) isotropic FGM plates; (ii) sandwich plates with FGM face sheets and homogeneous core; (iii) sandwich plates with homogeneous face sheets and FGM core. The material properties of FGM sandwich plates are varied according to a power-law function. To assess the performance and reliability of the present layerwise FE model, several examples covering the various features such as effects of material distribution, side to-thickness ratio, aspect ratios, core-to-face thickness ratio, boundary conditions, volume fraction index, are solved for symmetric and non-symmetric FGM sandwich plates. Effects of hardcore and softcore on the non-dimensional natural frequencies are discussed as well. The author's results are compared with those obtained using the 3D exact elasticity theory, refined analytical solutions and other advanced finite element models. Finally, the new results obtained from this study are provided as a benchmark for future investigations.

## 2 Theoretical formulation

### 2.1 Geometrical configuration

A rectangular isotropic FGM plates is considered as shown in Fig. 1. The plate has length  $a$ , width  $b$ , and thickness  $h$ . The mid-plane of the plate ( $z=0$ ) is considered as the

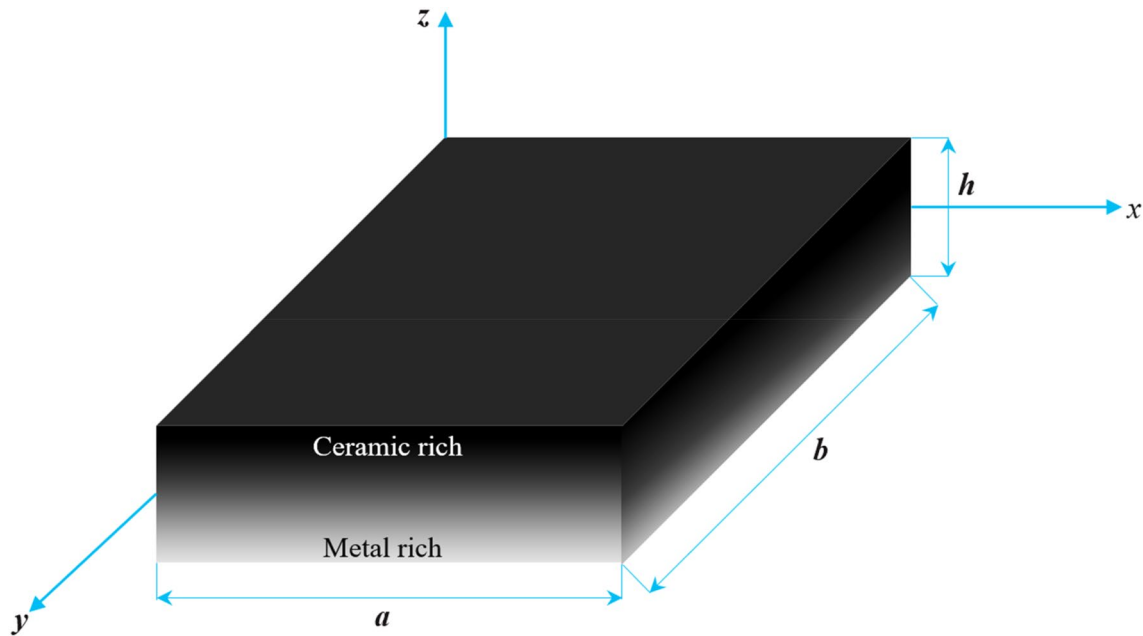


Fig. 1 Geometry of a typical FGM plate (Type A)

reference plane. In the present study, three types of FGM plates are studied: (A) isotropic FGM plates; (B) sandwich plates with homogeneous face sheets and FGM core; (C) sandwich plates with FGM face sheets and homogeneous core.

2.1.1 Type A: isotropic FGM plates

The plate is graded from a mixture of metal and ceramic, in which the composition is varied from the top to the bottom surface (see Fig. 1). The volume fraction of the FGM plate vary along the thickness direction via a power-law function as follows [67]:

$$V_c(z) = \left( \frac{2z + h}{2h} \right)^k, z \in [-h/2, h/2] \tag{1}$$

where the volume fractions of the ceramic ( $V_c$ ) and the metal ( $V_m$ ) phases are related by  $V_c + V_m = 1$ .  $k$  is the volume fraction index ( $0 \leq k \leq +\infty$ ) that allows the user to define gradation of material properties through the thickness direction. The value of ‘ $k$ ’ equal to 0 and  $+\infty$  represents a fully ceramic and metal plate, respectively.

2.1.2 Type B: sandwich plates with homogeneous face sheets and FGM core.

In this type, the top and bottom face sheet, of thickness ( $h_t$ ) and ( $h_b$ ), are made of pure ceramic and metal, respectively, while the FGM core layer, of thickness ( $h_c$ ), is graded from metal to ceramic (see Fig. 2). Thus, there are no interfaces between core and face sheets.

The vertical positions of the bottom surface, the two interfaces between the layers, and the top surface are denoted by  $h_1 = h/2, h_2, h_3$ , and  $h_4 = -h/2$ , respectively. The volume fraction of each component material is defined as:

$$\begin{aligned} V_1(z) &= 1 \text{ for } z \in [h_3, h_4], \text{ Top face sheet;} \\ V_2(z) &= \left( \frac{z - h_2}{h_3 - h_2} \right)^k \text{ for } z \in [h_2, h_3], \text{ Core;} \\ V_3(z) &= 0 \text{ for } z \in [h_1, h_2], \text{ Bottom face sheet} \end{aligned} \tag{2}$$

Here  $h_1 = -(h_c/2 + h_b), h_2 = -h_c/2, h_3 = h_c/2, h_4 = (h_t + h_c/2)$  as shown in Fig. 2.

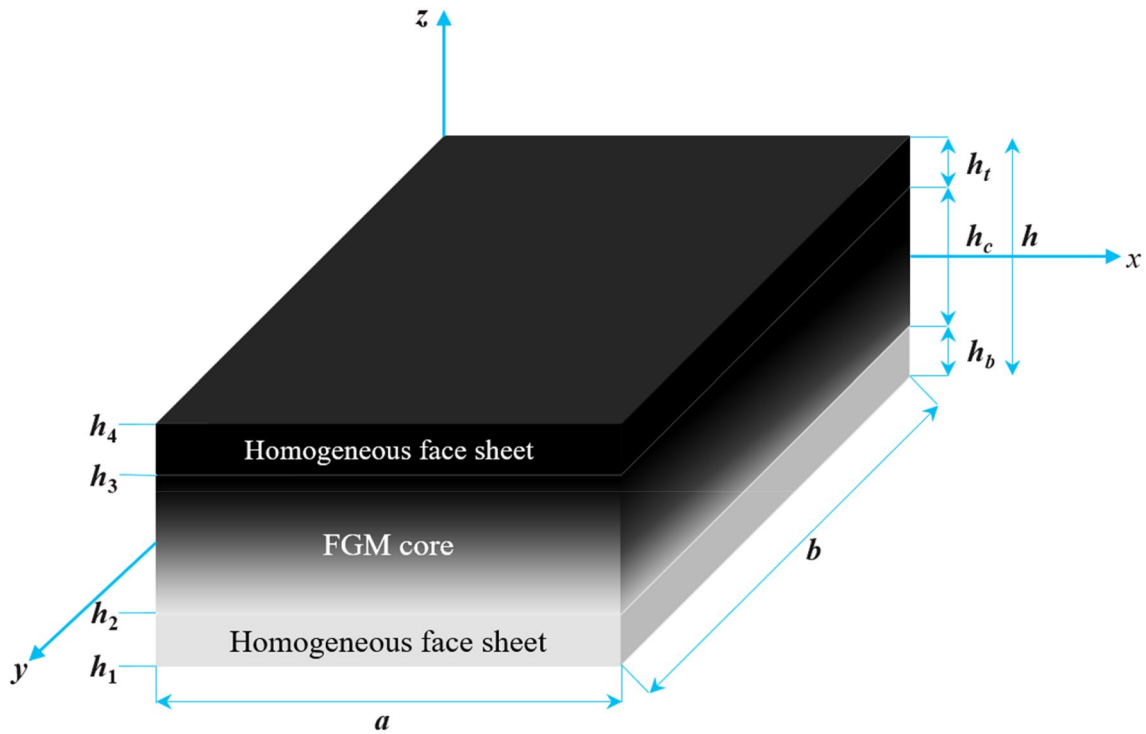


Fig. 2 Geometry of the sandwich plate with FGM core and homogenous face sheets (Type B)

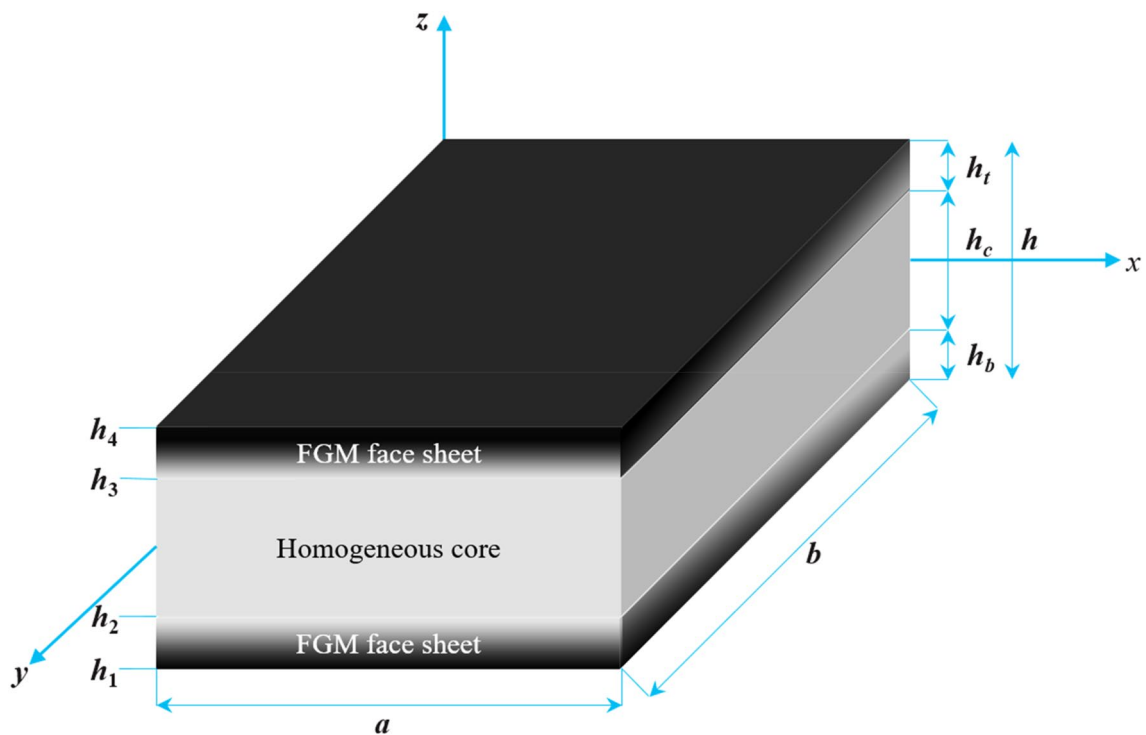


Fig. 3 Geometry of the sandwich plate with FGM face sheets and homogenous core (Type C)

### 2.1.3 Type C: sandwich plates with FGM face sheets and homogeneous core

As shown in Fig. 3, the top and bottom face sheets are assumed as FGM through the thickness direction, whereas the core is made of an isotropic homogeneous material. In this case, the volume fraction of the FGM sandwich plate can be expressed as [3, 23]:

$$\begin{aligned}
 V_1(z) &= \left(\frac{z - h_4}{h_3 - h_4}\right)^k \text{ for } z \in [h_3, h_4], \text{ Top face sheet;} \\
 V_2(z) &= 1 \text{ for } z \in [h_2, h_3], \text{ Core;} \\
 V_3(z) &= \left(\frac{z - h_1}{h_2 - h_1}\right)^k \text{ for } z \in [h_1, h_2], \text{ Bottom face sheet}
 \end{aligned}
 \tag{3}$$

Figure 4 show the through thickness variation of the volume fraction function of the mentioned three cases of FGM plates for various values of the power law index  $k$ .

### 2.2 Estimation of mechanical properties

The effective material properties of the plate, which are assumed to varying smoothly across the thickness direction due to a power-law distribution, are calculated using the following rule of mixture [68]:

$$P^{(n)}(z) = P_2 + (P_1 - P_2)V^{(n)}
 \tag{4}$$

where  $P^{(n)}(z)$  represents the effective material properties for each layer  $n$  ( $n = 1, 2, 3$ ), viz., Young’s modulus  $E$ , Poisson’s ratio  $\nu$ , and mass density  $\rho$ .  $V^{(n)}$  is the volume fraction of each layer depends on the type of FGM plate. For type B,  $P_1$  and  $P_2$  are the properties of the top and bottom faces of layer 1 ( $h_1 \leq z \leq h_2$ ), respectively, and vice versa for layer 3 ( $h_3 \leq z \leq h_4$ ) depending on the volume fraction. For type C,  $P_1$  and  $P_2$  are the properties of layer 3 and layer 1, respectively. For simplicity, Poisson’s ratio of plate is assumed to be constant in this study for that the effect of Poisson’s ratio on deformation is much less than that of Young’s modulus [69].

### 2.3 Kinematics of the present layerwise model

#### 2.3.1 Displacement field

In the present layerwise model, the HSDT is adopted for the core layer. Hence, the displacements fields are written as a cubic pattern for the in-plane displacements, and as a constant one for the transverse displacement:

$$\begin{aligned}
 u_c &= u_0 + z\psi_x^c + z^2\eta_x^c + z^3\zeta_x^c \\
 v_c &= v_0 + z\psi_y^c + z^2\eta_y^c + z^3\zeta_y^c \\
 w_c &= w_0
 \end{aligned}
 \tag{5}$$

where  $u_0, v_0$  and  $w_0$  are respectively, in-plane and transverse displacement components at the mid-plane of the sandwich plate.  $\psi_x^c, \psi_y^c$  represent normal rotations about the  $x$  and  $y$  axis, respectively. The parameters  $\eta_x^c, \eta_y^c, \zeta_x^c$  and  $\zeta_y^c$  are higher order terms.

The FSDT is adopted to model the top and bottom face sheet. The compatibility conditions as well as the displacement continuity between the face sheets and the core, which is assumed to be perfect, leads to the following improved displacement fields (Fig. 5):

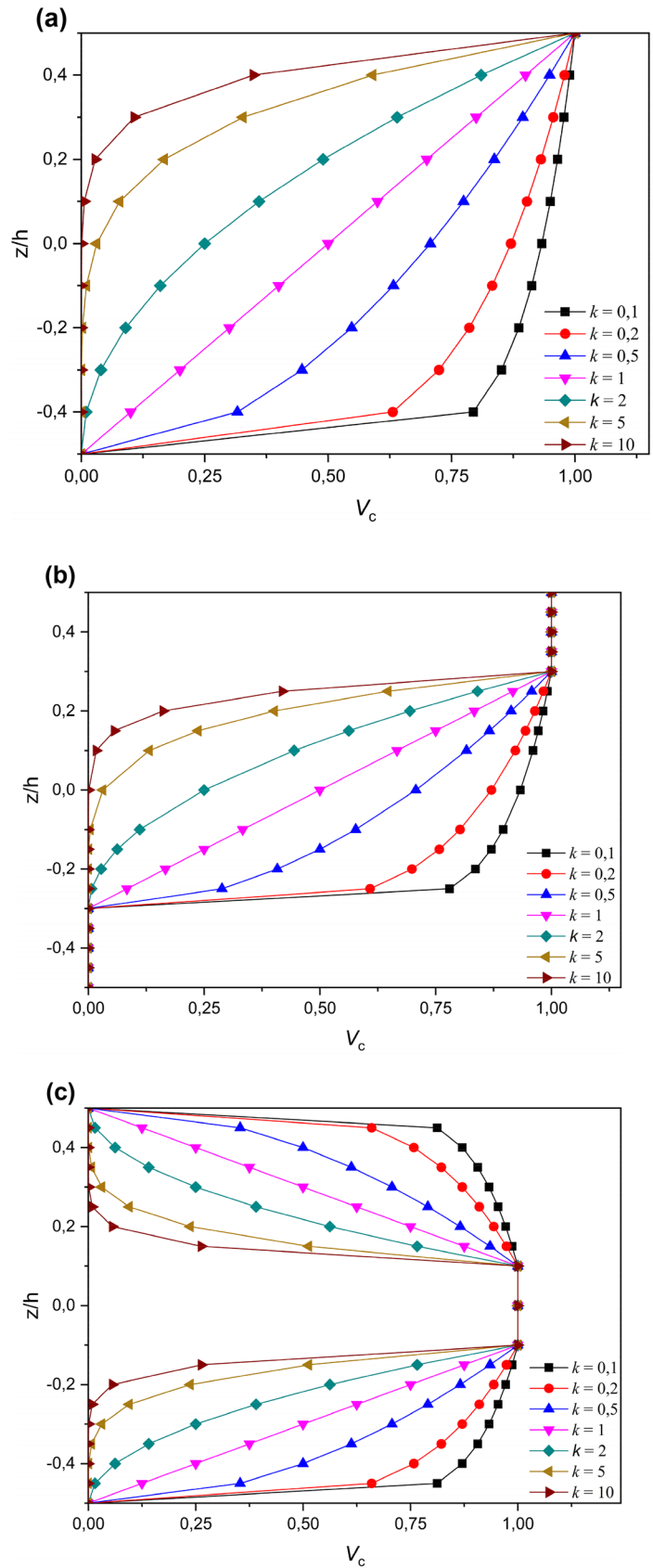
- Top face sheet

$$\begin{aligned}
 u_t &= u_0 + \left(\frac{h_c}{2}\right)\psi_x^c + \left(\frac{h_c^2}{4}\right)\eta_x^c + \left(\frac{h_c^3}{8}\right)\zeta_x^c + \left(z - \frac{h_c}{2}\right)\psi_x^t \\
 v_t &= v_0 + \left(\frac{h_c}{2}\right)\psi_y^c + \left(\frac{h_c^2}{4}\right)\eta_y^c + \left(\frac{h_c^3}{8}\right)\zeta_y^c + \left(z - \frac{h_c}{2}\right)\psi_y^t \\
 w_t &= w_0
 \end{aligned}
 \tag{6}$$

where  $\psi_x^t$  and  $\psi_y^t$  are the rotations of the top face-sheet cross section about the  $y$  and  $x$  axis, respectively.

- Bottom face sheet

**Fig. 4** Variation of volume fraction of the ceramic constituent through the thickness of three types of FGM plates for various values of the power law index  $k$ : **a** Type (A), **b** Type (B) and **c** Type C



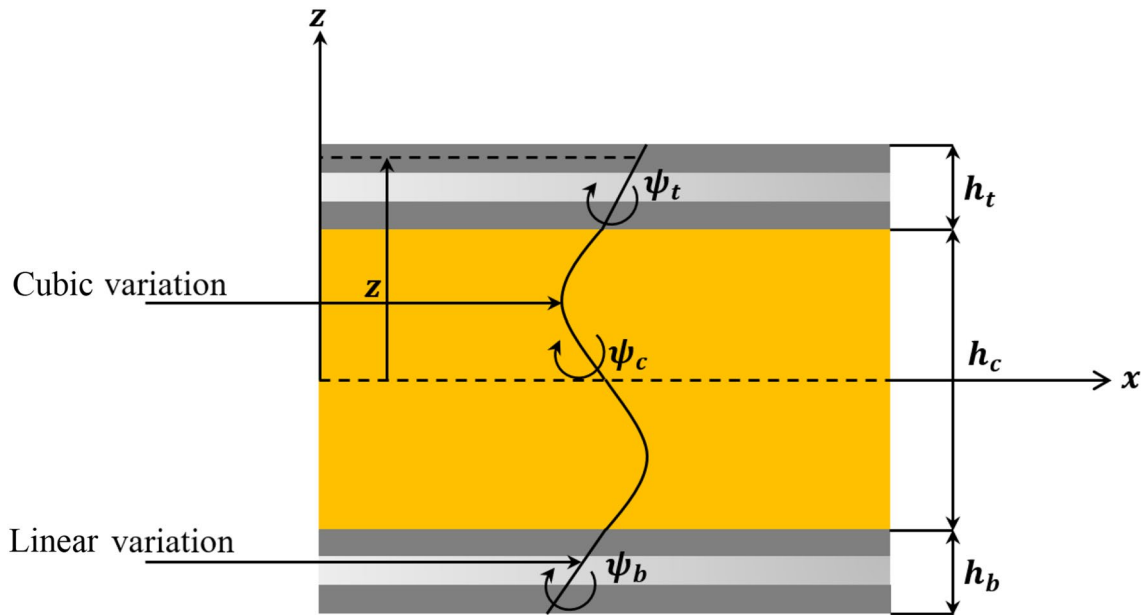


Fig. 5 Representation of layerwise kinematics and coordinate system

$$\begin{aligned}
 u_b &= u_0 - \left(\frac{h_c}{2}\right)\psi_x^c + \left(\frac{h_c^2}{4}\right)\eta_x^c - \left(\frac{h_c^3}{8}\right)\zeta_x^c + \left(z + \frac{h_c}{2}\right)\psi_x^b \\
 v_b &= v_0 - \left(\frac{h_c}{2}\right)\psi_y^c + \left(\frac{h_c^2}{4}\right)\eta_y^c - \left(\frac{h_c^3}{8}\right)\zeta_y^c + \left(z + \frac{h_c}{2}\right)\psi_y^b \\
 w_b &= w_0
 \end{aligned}
 \tag{7}$$

where  $\psi_x^b$  and  $\psi_y^b$  are the rotations of the bottom face-sheet cross section about the y and x axis, respectively.

### 2.3.2 Strain–displacement relations

The strain–displacement relations corresponding to any *i*th (*i* = 1, 2, 3) layer of FGM sandwich plate are given as follows:

For the core layer,

$$\begin{aligned}
 \epsilon_{xx}^c &= \frac{\partial u_0}{\partial x} + z \frac{\partial \psi_x^c}{\partial x} + z^2 \frac{\partial \eta_x^c}{\partial x} + z^3 \frac{\partial \zeta_x^c}{\partial x} \\
 \epsilon_{yy}^c &= \frac{\partial v_0}{\partial y} + z \frac{\partial \psi_y^c}{\partial y} + z^2 \frac{\partial \eta_y^c}{\partial y} + z^3 \frac{\partial \zeta_y^c}{\partial y} \\
 \gamma_{xy}^c &= \left(\frac{\partial u_0}{\partial y} + \frac{\partial v_0}{\partial x}\right) + z \left(\frac{\partial \psi_x^c}{\partial y} + \frac{\partial \psi_y^c}{\partial x}\right) + z^2 \left(\frac{\partial \eta_x^c}{\partial y} + \frac{\partial \eta_y^c}{\partial x}\right) + z^3 \left(\frac{\partial \zeta_x^c}{\partial y} + \frac{\partial \zeta_y^c}{\partial x}\right) \\
 \gamma_{yz}^c &= \psi_y^c + \frac{\partial w_0}{\partial y} + 2z\eta_y^c + 3z^2\zeta_y^c \\
 \gamma_{xz}^c &= \psi_x^c + \frac{\partial w_0}{\partial x} + 2z\eta_x^c + 3z^2\zeta_x^c
 \end{aligned}
 \tag{8}$$



For the top face sheet,

$$\begin{aligned}
 \epsilon_{xx}^t &= \frac{\partial u_t}{\partial x} = \frac{\partial u_0}{\partial x} + \left(\frac{h_c}{2}\right) \frac{\partial \psi_x^c}{\partial x} + \left(\frac{h_c^2}{4}\right) \frac{\partial \eta_x^c}{\partial x} + \left(\frac{h_c^3}{8}\right) \frac{\partial \zeta_x^c}{\partial x} + \left(z - \frac{h_c}{2}\right) \frac{\partial \psi_x^t}{\partial x} \\
 \epsilon_{yy}^t &= \frac{\partial v_t}{\partial y} = \frac{\partial v_0}{\partial x} + \left(\frac{h_c}{2}\right) \frac{\partial \psi_y^c}{\partial y} + \left(\frac{h_c^2}{4}\right) \frac{\partial \eta_y^c}{\partial y} + \left(\frac{h_c^3}{8}\right) \frac{\partial \zeta_y^c}{\partial y} + \left(z - \frac{h_c}{2}\right) \frac{\partial \psi_y^t}{\partial y} \\
 \gamma_{xy}^t &= \frac{\partial u_t}{\partial y} + \frac{\partial v_t}{\partial x} = \left(\frac{\partial u_0}{\partial y} + \frac{\partial v_0}{\partial x}\right) + \frac{h_c}{2} \left(\frac{\partial \psi_x^c}{\partial y} + \frac{\partial \psi_y^c}{\partial x}\right) + \frac{h_c^2}{4} \left(\frac{\partial \eta_x^c}{\partial y} + \frac{\partial \eta_y^c}{\partial x}\right) \\
 &\quad + \frac{h_c^3}{8} \left(\frac{\partial \zeta_x^c}{\partial y} + \frac{\partial \zeta_y^c}{\partial x}\right) + \left(z - \frac{h_c}{2}\right) \left(\frac{\partial \psi_x^t}{\partial y} + \frac{\partial \psi_y^t}{\partial x}\right) \\
 \gamma_{yz}^t &= \frac{\partial w_0}{\partial y} + \psi_y^t \\
 \gamma_{xz}^t &= \frac{\partial w_0}{\partial x} + \psi_x^t
 \end{aligned} \tag{9}$$

We follow the same procedure for strain–displacement relations of the bottom face sheet.

### 2.4 Constitutive equations

The stress–strain relationship of FGM sandwich plate, for three layers ( $n = 1, 2, 3$ ), is given by:

$$\begin{Bmatrix} \sigma_{xx} \\ \sigma_{yy} \\ \sigma_{yz} \\ \sigma_{xz} \\ \sigma_{xy} \end{Bmatrix}^{(n)} = \begin{bmatrix} Q_{11} & Q_{12} & 0 & 0 & 0 \\ Q_{21} & Q_{22} & 0 & 0 & 0 \\ 0 & 0 & Q_{44} & 0 & 0 \\ 0 & 0 & 0 & Q_{55} & 0 \\ 0 & 0 & 0 & 0 & Q_{66} \end{bmatrix}^{(n)} \begin{Bmatrix} \epsilon_{xx} \\ \epsilon_{yy} \\ \gamma_{yz} \\ \gamma_{xz} \\ \gamma_{xy} \end{Bmatrix}^{(n)} \tag{10}$$

where  $Q_{ij}$  is the stiffness coefficient matrix, which are functions of coordinate  $z$ , defined as:

$$\begin{aligned}
 Q_{11} = Q_{22} &= \frac{E(z)}{1 - \nu^2(z)}, \quad Q_{12} = Q_{21} = \nu(z)Q_{11}, \quad Q_{44} = Q_{55} = \\
 Q_{66} &= \frac{E(z)}{2(1 - \nu(z))}
 \end{aligned}$$

For the core layer, the efforts resultants are obtained by integration of the stresses through the thickness direction of laminated plate.

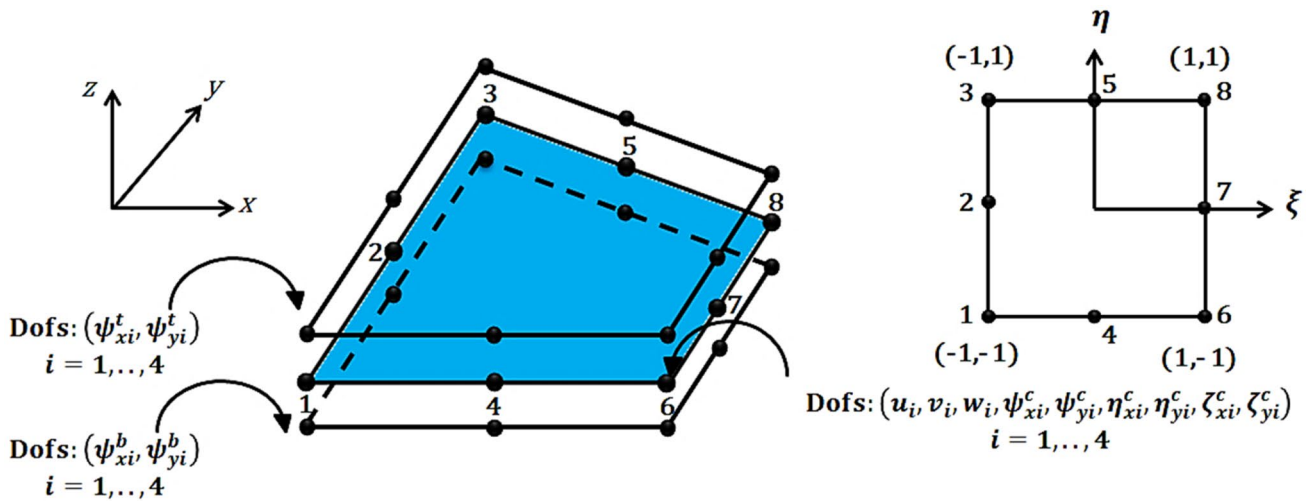


Fig. 6 Geometry and corresponding DOFs of the present element

$$\begin{bmatrix} N_x & M_x & \overline{N}_x & \overline{M}_x \\ N_y & M_y & \overline{N}_y & \overline{M}_y \\ N_{xy} & M_{xy} & \overline{N}_{xy} & \overline{M}_{xy} \end{bmatrix} = \int_{-\frac{h_c}{2}}^{\frac{h_c}{2}} \begin{Bmatrix} \sigma_x \\ \sigma_y \\ \tau_{xy} \end{Bmatrix} (1, z, z^2, z^3) dz \tag{11}$$

$$\begin{bmatrix} V_x & S_x & R_x \\ V_y & S_y & R_y \end{bmatrix} = \int_{-\frac{h_c}{2}}^{\frac{h_c}{2}} \begin{Bmatrix} \tau_{xz} \\ \tau_{yz} \end{Bmatrix} (1, z, z^2) dz$$

where  $N$  and  $M$  denote membrane and bending moment, respectively, and  $\overline{N}$  and  $\overline{M}$  are the higher order moment resultants.  $V$  is the shear resultant;  $S$  and  $R$  are the higher order shear resultant.

Substituting Eq. (10) into Eq. (11) and integrating through the thickness of the plate, the stress resultants of the core are given as:

$$\begin{Bmatrix} N \\ M \\ \overline{N} \\ \overline{M} \end{Bmatrix} = \begin{bmatrix} [A] & [B] & [D] & [E] \\ [B] & [D] & [E] & [F] \\ [D] & [E] & [F] & [G] \\ [E] & [F] & [G] & [H] \end{bmatrix} \begin{Bmatrix} \epsilon^{(0)} \\ \chi^{(1)} \\ \chi^{(2)} \\ \chi^{(3)} \end{Bmatrix} \tag{12a}$$

$$\begin{Bmatrix} V \\ S \\ R \end{Bmatrix} = \begin{bmatrix} [A^s] & [B^s] & [D^s] \\ [B^s] & [D^s] & [E^s] \\ [D^s] & [E^s] & [F^s] \end{bmatrix} \begin{Bmatrix} \gamma_s^{(0)} \\ \chi_s^{(1)} \\ \chi_s^{(2)} \end{Bmatrix} \tag{12b}$$

where  $[A_{ij}]$ ,  $[B_{ij}]$  are the elements of the reduced stiffness matrices of the core, defined by:

$$(A_{ij}, B_{ij}, D_{ij}, E_{ij}, F_{ij}, G_{ij}, H_{ij}) = \int_{-\frac{h_c}{2}}^{\frac{h_c}{2}} Q_{ij}(z) (1, z, z^2, z^3, z^4, z^5, z^6) dz (i, j = 1, 2, 6) \tag{13}$$

$$(A_{ij}^s, B_{ij}^s, D_{ij}^s, E_{ij}^s, F_{ij}^s) = \int_{-\frac{h_c}{2}}^{\frac{h_c}{2}} Q_{ij}(z) (1, z, z^2, z^3, z^4) dz (i, j = 4, 5)$$

According to the FSDT, the constitutive equations for the two face sheets are:

$$\begin{Bmatrix} N^f \\ M^f \\ T^f \end{Bmatrix} = \begin{bmatrix} A^f & B^f & 0 \\ B^f & D^f & 0 \\ 0 & 0 & A_c^f \end{bmatrix} \begin{Bmatrix} \epsilon_m^f \\ \epsilon_f^f \\ \gamma_c^f \end{Bmatrix} \tag{14}$$

where the elements of reduced stiffness matrices of the face sheets are given by:

- Top face sheet

$$(A_{ij}^t, B_{ij}^t, D_{ij}^t) = \int_{\frac{h_c}{2}}^{\frac{h_c}{2}+h_t} Q_{ij}(z) (1, z, z^2) dz (i, j = 1, 2, 6) \tag{15}$$

$$(\overline{A}_{ij}^t) = \int_{\frac{h_c}{2}}^{\frac{h_c}{2}+h_t} Q_{ij}(z) dz (i, j = 4, 5)$$

- Bottom face sheet

$$(A_{ij}^b, B_{ij}^b, D_{ij}^b) = \int_{-(\frac{h_c}{2}+h_b)}^{-\frac{h_c}{2}} Q_{ij}(z) (1, z, z^2) dz (i, j = 1, 2, 6) \tag{16}$$

$$(\overline{A}_{ij}^b) = \int_{-(\frac{h_c}{2}+h_b)}^{-\frac{h_c}{2}} Q_{ij}(z) dz (i, j = 4, 5)$$

### 3 Finite element formulation

In the present work, a  $C^0$  eight-node isoparametric element, denoted FEM-Q8-LW, with 13 DOFs per node is developed for free vibration of functionally graded sandwich plates. This new element is formulated based on recently proposed layerwise model. Each node contains: two rotational DOFs for each face sheet, six rotational DOFs for the core, while the three translations DOFs are common for sandwich layers (Fig. 6). One of the characteristic features of the element is imposed the same transverse displacement of each layer. Hence, the number of variables is fixed and does not increase when increasing the number of layers. The proposed model can provide more accu-

rate results for symmetric and non-symmetric thin/thick FGM sandwich plate with various boundary conditions and arbitrary FG material distribution. Further, the numerical results show that the present finite element model is free of shear locking and have a high accuracy and fast rate of convergence.

The displacements vectors at any point of coordinates  $(x, y)$  of the plate are given by:

$$\delta(x, y) = \sum_{i=1}^8 N_i \delta_i \tag{17}$$

where  $\delta_i = \{u_{0i} \ v_{0i} \ w_{0i} \ \psi_{xi}^c \ \psi_{yi}^c \ \eta_{xi}^c \ \eta_{yi}^c \ \zeta_{xi}^c \ \zeta_{yi}^c \ \psi_{xi}^t \ \psi_{yi}^t \ \psi_{xi}^b \ \psi_{yi}^b\}^T$  is the displacement vector corresponding to node  $i$  ( $i = 1-8$ ).  $N_i$  are the classical serendipity interpolation functions which given as:

$$\begin{aligned} N_1(\xi, \eta) &= \frac{1}{4}(1 - \xi)(\eta - 1)(\xi + \eta + 1), \quad N_2(\xi, \eta) = \frac{1}{4}(1 + \xi)(\eta - 1)(-\xi + \eta + 1) \\ N_3(\xi, \eta) &= \frac{1}{4}(1 + \xi)(\eta + 1)(\xi + \eta - 1), \quad N_4(\xi, \eta) = \frac{1}{4}(-1 + \xi)(\eta + 1)(\xi - \eta + 1) \\ N_5(\xi, \eta) &= \frac{1}{2}(1 - \eta)(1 - \xi^2), \quad N_6(\xi, \eta) = \frac{1}{2}(1 - \eta^2)(1 + \xi) \\ N_7(\xi, \eta) &= \frac{1}{2}(1 + \eta)(1 - \xi^2), \quad N_8(\xi, \eta) = \frac{1}{2}(1 - \eta^2)(1 - \xi) \end{aligned} \tag{18}$$

The generalized strain vector for three layers can be expressed in terms of nodal displacements vector as follows:

$$\{\epsilon^{(k)}\} = [B_i^{(k)}] \{\delta_i\} \tag{19}$$

where the matrices  $[B_i^{(k)}]$  relate the strains to nodal displacements.

### 4 Governing differential equation

In this work, Hamilton’s principle is applied to formulate governing equation for the bending and free vibration analyses of FGM sandwich plate, which is given as:

$$\delta \Pi = \int_{t_1}^{t_2} \delta(U + W - T) dt = 0 \tag{20}$$

where  $t$  is the time,  $U$  is the strain energy,  $W$  is the work done due to external force and  $T$  is the kinetic energy.

The variation of strain energy of FGM sandwich plate is the summation of contribution from the two face sheets and from the core as:

$$\begin{aligned} \delta U &= \int_{A_c} \int_{-\frac{h_c}{2}}^{\frac{h_c}{2}} \left( \sigma_{xx}^c \delta \epsilon_{xx}^c + \sigma_{yy}^c \delta \epsilon_{yy}^c + \sigma_{xy}^c \delta \epsilon_{xy}^c + \sigma_{xz}^c \delta \epsilon_{xz}^c + \sigma_{yz}^c \delta \epsilon_{yz}^c \right) dV_c \\ &+ \int_{A_t} \int_{\frac{h_c}{2}}^{\frac{h_c}{2} + h_t} \left( \sigma_{xx}^t \delta \epsilon_{xx}^t + \sigma_{yy}^t \delta \epsilon_{yy}^t + \sigma_{xy}^t \delta \epsilon_{xy}^t + \sigma_{xz}^t \delta \epsilon_{xz}^t + \sigma_{yz}^t \delta \epsilon_{yz}^t \right) dV_t \\ &+ \int_{A_b} \int_{-\frac{h_c}{2} - h_b}^{-\frac{h_c}{2}} \left( \sigma_{xx}^b \delta \epsilon_{xx}^b + \sigma_{yy}^b \delta \epsilon_{yy}^b + \sigma_{xy}^b \delta \epsilon_{xy}^b + \sigma_{xz}^b \delta \epsilon_{xz}^b + \sigma_{yz}^b \delta \epsilon_{yz}^b \right) dV_b \end{aligned} \tag{21}$$

The work done by external transverse static load of intensity  $f(x, y)$  on  $j^{th}$  element is

$$\delta W = \int_A f(x, y)_j \delta w dA \tag{22}$$

where  $f_j$  is the nodal load vector corresponding to  $j$ th

element.

The variation of kinetic energy for an  $i$ th layer of a FGM sandwich plate can be expressed as:

$$\begin{aligned} \delta T &= \int_{V_t} \rho_t(z) (\ddot{u}_t \delta u_t + \ddot{v}_t \delta v_t + \ddot{w}_t \delta w_t) dV_t \\ &+ \int_{V_c} \rho_c(z) (\ddot{u}_c \delta u_c + \ddot{v}_c \delta v_c + \ddot{w}_c \delta w_c) dV_c \\ &+ \int_{V_b} \rho_b(z) (\ddot{u}_b \delta u_b + \ddot{v}_b \delta v_b + \ddot{w}_b \delta w_b) dV_b \end{aligned} \tag{23}$$

where  $u_i, v_i$  and  $w_i$  are the displacement in  $x, y$  and  $z$  directions, respectively, of the three-layered sandwich ( $i = t, c, b$ ),  $\rho_i(z)$  are the effective density of the FGM sandwich plate, and  $(..)$  is a second derivative with respect to time.

- Kinetic energy of the core

From the displacement field of the core, defined by Eq. (5), the kinetic energy of the core can be expressed as:

$$\begin{aligned} \delta T_c &= \int_{\Omega_0} \left[ I_0 (\ddot{u}_0 \delta u_0 + \ddot{v}_0 \delta v_0 + \ddot{w}_0 \delta w_0) + I_1 (\ddot{u}_0 \delta \psi_x^c + \ddot{\psi}_x^c \delta u_0 + \ddot{v}_0 \delta \psi_y^c + \ddot{\psi}_y^c \delta v_0) \right. \\ &+ I_2 (\ddot{u}_0 \delta \eta_x^c + \ddot{\psi}_x^c \delta \psi_x^c + \ddot{\eta}_x^c \delta u_0 + \ddot{v}_0 \delta \eta_y^c + \ddot{\psi}_y^c \delta \psi_y^c + \ddot{\eta}_y^c \delta v_0) \\ &+ I_3 (\ddot{u}_0 \delta \zeta_x^c + \ddot{\psi}_x^c \delta \eta_x^c + \ddot{\eta}_x^c \delta \psi_x^c + \ddot{\zeta}_x^c \delta u_0 + \ddot{v}_0 \delta \zeta_y^c + \ddot{\psi}_y^c \delta \eta_y^c + \ddot{\eta}_y^c \delta \psi_y^c + \ddot{\zeta}_y^c \delta v_0) \\ &+ I_4 (\ddot{\psi}_x^c \delta \zeta_x^c + \ddot{\eta}_x^c \delta \eta_x^c + \ddot{\zeta}_x^c \delta \psi_x^c + \ddot{\psi}_y^c \delta \zeta_y^c + \ddot{\eta}_y^c \delta \eta_y^c + \ddot{\zeta}_y^c \delta \psi_y^c) \\ &+ I_5 (\ddot{\eta}_x^c \delta \zeta_x^c + \ddot{\zeta}_x^c \delta \eta_x^c + \ddot{\eta}_y^c \delta \zeta_y^c + \ddot{\zeta}_y^c \delta \eta_y^c) + I_6 (\ddot{\zeta}_x^c \delta \zeta_x^c + \ddot{\zeta}_y^c \delta \zeta_y^c) \Big] dx dy \end{aligned} \tag{24}$$

where the inertia moments of the core  $I_i = (i = 0-6)$  are defined by:

$$(I_0, I_1, I_2, I_3, I_4, I_5, I_6) = \int_{-\frac{h_c}{2}}^{\frac{h_c}{2}} \rho_c(z) (1, z, z^2, z^3, z^4, z^5, z^6) dz \tag{25}$$

We follow the same procedure for kinetic energy of the face sheets.

For linear static analysis, the equilibrium equation can be expressed as follows:

$$[K] = \{\delta\} \{F\} \tag{26}$$

where  $\{F\}$  and  $[K_e]$  are the load vector and the element stiffness matrix of the plate, respectively.

For free vibration problem, the work done by external forces and the damping are neglected. The Hamilton’s principle (Eq. 20) leads to the following dynamic equilibrium equation of a system.

$$[M_e] \{\ddot{\delta}\} + [K_e] \{\delta\} = 0 \tag{27}$$

where  $[M_e]$  and  $[K_e]$  denote the total element mass matrix and the total element stiffness matrix respectively, which are computed using the Gauss numerical integration.

The total element stiffness matrix is the summation of contribution from the two face sheets and from the core as:

$$[K_e] = [K_e^{(t)}] + [K_e^{(c)}] + [K_e^{(b)}] \tag{28}$$

where the element stiffness matrix of the two face sheet is given by:

a. Top face sheet:

$$[K_e^{(t)}] = \iint \left( \underbrace{[B_m^t]^T [A^{(t)}] [B_m^t]}_{\text{membrane}} + \underbrace{[B_m^t]^T [B^{(t)}] [B_f^t]}_{\text{coupling membrane - bending}} + \underbrace{[B_f^t]^T [B^{(t)}] [B_m^t]}_{\text{coupling bending - membrane}} + \underbrace{[B_f^t]^T [D^{(t)}] [B_f^t]}_{\text{bending}} + \underbrace{[B_s^t]^T [A_c^{(t)}] [B_s^t]}_{\text{shear}} \right) dA \tag{29}$$

b. Bottom face sheet:

$$[K_e^{(b)}] = \iint \left( \underbrace{[B_m^b]^T [A^{(b)}] [B_m^b]}_{\text{membrane}} + \underbrace{[B_m^b]^T [B^{(b)}] [B_f^b]}_{\text{coupling membrane - bending}} + \underbrace{[B_f^b]^T [B^{(b)}] [B_m^b]}_{\text{coupling bending - membrane}} + \underbrace{[B_f^b]^T [D^{(b)}] [B_f^b]}_{\text{bending}} + \underbrace{[B_s^b]^T [A_c^{(b)}] [B_s^b]}_{\text{shear}} \right) dA \tag{30}$$

For the core, the element stiffness matrix can be written as:

$$[K_e^{(c)}] = \iint \left( [B_\epsilon^{(0)}]^T [A] [B_\epsilon^{(0)}] + [B_\epsilon^{(0)}]^T [B] [B_\chi^{(1)}] + [B_\epsilon^{(0)}]^T [D] [B_\chi^{(2)}] + [B_\epsilon^{(0)}]^T [E] [B_\chi^{(3)}] + [B_\chi^{(1)}]^T [B] [B_\epsilon^{(0)}] + [B_\chi^{(1)}]^T [D] [B_\epsilon^{(0)}] + [B_\chi^{(1)}]^T [E] [B_\chi^{(2)}] + [B_\chi^{(1)}]^T [F] [B_\chi^{(3)}] + [B_\chi^{(2)}]^T [D] [B_\epsilon^{(0)}] + [B_\chi^{(2)}]^T [E] [B_\chi^{(1)}] + [B_\chi^{(2)}]^T [F] [B_\chi^{(2)}] + [B_\chi^{(2)}]^T [L] [B_\chi^{(3)}] + [B_\chi^{(3)}]^T [E] [B_\epsilon^{(0)}] + [B_\chi^{(3)}]^T [F] [B_\chi^{(1)}] + [B_\chi^{(3)}]^T [L] [B_\chi^{(2)}] + [B_\chi^{(3)}]^T [H] [B_\chi^{(3)}] + [B_{\gamma_s}^{(0)}]^T [A^s] [B_{\gamma_s}^{(0)}] + [B_{\gamma_s}^{(0)}]^T [B^s] [B_{\chi_s}^{(1)}] + [B_{\gamma_s}^{(0)}]^T [D^s] [B_{\chi_s}^{(2)}] + [B_{\chi_s}^{(1)}]^T [B^s] [B_{\gamma_s}^{(0)}] + [B_{\chi_s}^{(1)}]^T [D^s] [B_{\chi_s}^{(1)}] + [B_{\chi_s}^{(1)}]^T [E^s] [B_{\chi_s}^{(2)}] + [B_{\chi_s}^{(2)}]^T [D^s] [B_{\gamma_s}^{(0)}] + [B_{\chi_s}^{(2)}]^T [E^s] [B_{\chi_s}^{(1)}] + [B_{\chi_s}^{(2)}]^T [F^s] [B_{\chi_s}^{(2)}] \right) dA \tag{31}$$

The total element mass matrix, for the three-layer sandwich plate, can be written as

$$[M_e] = \iint \left( [N]^T [m^{(t)}] [N] + [N]^T [m^{(c)}] [N] + [N]^T [m^{(b)}] [N] \right) dA \tag{32}$$

where  $[m^{(t)}]$ ,  $[m^{(c)}]$  and  $[m^{(b)}]$  are the consistent mass matrices

of the top face sheet, core and the bottom face sheet, respectively, containing inertia terms.

Now, after evaluating the stiffness and mass matrices for all elements, the governing equations for free vibration analysis of FGM sandwich plate can be stated in the form of generalized eigenvalue problem.

$$[K]\{\chi\} - \omega^2[M]\{\chi\} = 0 \tag{33}$$

where,  $\omega$  denote the natural frequency,  $[K]$  is the global stiffness matrix,  $[M]$  is the global mass matrix,  $\{\chi\}$  are the vectors defining the mode shapes.

### 5 Numerical results and discussions

In this section, several numerical examples are presented and discussed to demonstrate the accuracy and robustness of the developed layerwise FE model in predicting the bending and free vibration responses of functionally graded sandwich plates. A wide range of comparison and convergence studies are presented with 2D/3D elasticity solutions and others finite elements numerical results found in the literature. The effect of different materials and

geometric parameters with arbitrary boundary conditions are carried-out in the present study. The applied boundary conditions and the material properties of FGM plates, considered for all examples, are illustrated in Tables 1 and 2, respectively.

Several kinds of FGM sandwich plates are considered for presenting the numerical results.

- The (1-1-1) FGM sandwich plate: the plate is symmetric and made of three equal-thickness layers.
- The (1-0-1) FGM sandwich plate: the plate is symmetric and made of two layers of equal thickness without a core.
- The (2-1-2) FGM sandwich plate: the core has half the thickness of the functionally graded face sheets.
- The (1-2-1) FGM sandwich plate: the functionally graded face sheets have half the thickness of the core.
- The (2-1-1) FGM sandwich plate: the plate is non-symmetric and here the core thickness equals the top face thickness while it is half the bottom face thickness.
- The (1-8-1) FGM sandwich plate: the core is eight times thicker than the individual face sheets.

**Table 1** Boundary conditions used in the present study

Boundary conditions	Abbreviations	Restrained edges
Simply supported	SSSS	$w_0 = \psi_x^c = \eta_x^c = \zeta_x^c = \psi_x^t = \psi_x^b = 0$ at $x = \pm a/2$ $w_0 = \psi_y^c = \eta_y^c = \zeta_y^c = \psi_y^t = \psi_y^b = 0$ at $x = \pm b/2$
Clamped	CCCC	$w_0 = \psi_x^c = \psi_y^c = \eta_x^c = \eta_y^c = \zeta_x^c = \zeta_y^c = \psi_x^t = \psi_y^t = \psi_x^b = \psi_y^b = 0$
Simply supported-Clamped	SCSC	Simply supported at $x = \pm a/2$ Clamped at $y = \pm b/2$
Simply supported-Free	SFSF	Simply supported at $x = \pm a/2$ Free at $y = \pm b/2$
Simply supported-Clamped-Free	SCSF	Simply supported at $x = \pm a/2$ Clamped at $y = -b/2$ , Free at $y = b/2$
Simply supported-Free	SSSF	Simply supported at $x = \pm a/2$ and $y = -b/2$ Free at $y = b/2$
Simply supported-Clamped	SSSC	Simply supported at $x = \pm a/2$ and $y = -b/2$ Clamped at $y = b/2$

**Table 2** Material properties used in the FG plate

Properties	Metal		Ceramic		
	Aluminum (Al*)	Aluminum (Al)	Alumina (Al <sub>2</sub> O <sub>3</sub> )	Zirconia (ZrO <sub>2</sub> -1)	Zirconia (ZrO <sub>2</sub> -2)
<i>E</i> (GPa)	70	70	380	200	151
$\nu$	0.3	0.3	0.3	0.3	0.3
$\rho$ (Knm/m <sup>3</sup> )	2702	2707	3800	5700	3000

### 5.1 Bending analysis

To verify the robustness and the accuracy of the proposed layerwise finite element formulation, it is necessary to validate it in the static analysis.

**Example 1** In the first example, the convergence test of the developed finite element is carried out for a square isotropic FGM plate subjected to uniformly distributed load. The single layered is made of aluminum and zirconia (Al/ZrO<sub>2</sub>) and their corresponding material properties are provided in Table 1. The top surface of FGM plate is ceramic-rich and the bottom surface is metal-rich. The study is performed for different volume fraction index (*k*) and boundary conditions with side-to-thickness ratio *a/h* = 5. The convergence of non-dimensional center deflections is reported in Table 3 for different mesh sizes (4 × 4, 6 × 6 and 8 × 8). The obtained results are compared with moving kriging (MK) meshfree methods based on HSDT [70], such as third shear deformation plate theory (TSDT), exponential shear deformation plate theory (ESDT) and inverse trigonometric shear deformation plate theory (ITSDT); and another HSDT model [71]

using more variables (18 DOFs/node). It is clear, for all the boundary conditions and the volume fraction index (*k*), that the present results are in good agreement with the existing solutions, as shown in Table 3. Thus, the performance of present finite element formulation is confirmed in terms of both accuracy and rate of convergence. Moreover, it can be clear, for all the applied boundary conditions (SFSF, SSSS and CCCC) that increasing the volume fraction index (*k*) results in an increase the central deflection (see Fig. 7). This behaviour is expected because the larger volume fraction index means the plate has a smaller ceramic component whose Young’s modulus is greater than that of metal and hence, the stiffness is reduced. In addition, it is evident that the central deflection decreases as the rigidity of boundary restraint is increased.

**Example 2.** This example is performed for symmetric and non-symmetric square FGM sandwich plate of type C. The face sheets are assumed to be made of FGM layers. The bottom face sheet are graded from metal to ceramic (Al/ZrO<sub>2</sub>) and the core layer is made of pure ceramic (ZrO<sub>2</sub>). The plate is fully clamped along their sides (CCCC) and

**Table 3** Non-dimensional center deflections ( $\bar{w}$ ) of Al/ZrO<sub>2</sub> FGM square plate subjected to uniformly distributed load with different boundary conditions and volume fraction index (*k*)

References	Models	<i>k</i>						
		Ceramic	0.5	1	2	4	8	Metal
Boundary conditions: SFSF								
Present element (4 × 4)	FEM-Q8-LW	0.5059 <sup>a</sup>	0.6921	0.8110	0.9299	1.0186	1.1017	1.4533
Present element (6 × 6)	FEM-Q8-LW	0.5057	0.6919	0.8108	0.9296	1.0182	1.1014	1.4538
Present element (8 × 8)	FEM-Q8-LW	0.5057	0.6919	0.8108	0.9295	1.0182	1.1013	1.4537
Gilhooley et al. [71]	HOSNDPT	0.5019	0.7543	0.8708	0.9744	–	–	1.4345
Nguyen et al. [70]	MK-TSDT	0.5098	0.7621	0.8793	0.9846	1.0717	1.1602	1.4563
	MK-ESDT	0.5089	0.7613	0.8791	0.9845	1.0714	1.1587	1.4553
	MK-ITSDT	0.5088	0.7609	0.8781	0.9840	1.0703	1.1576	1.4544
Boundary conditions: SSSS								
Present element (4 × 4)	FEM-Q8-LW	0.1705	0.2318	0.2716	0.3133	0.3467	0.3768	0.4899
Present element (6 × 6)	FEM-Q8-LW	0.1705	0.2322	0.2718	0.3134	0.3468	0.3770	0.4901
Present element (8 × 8)	FEM-Q8-LW	0.1706	0.2319	0.2718	0.3135	0.3468	0.3770	0.4901
Gilhooley et al. [71]	HOSNDPT	0.1671	0.2505	0.2905	0.3280	–	–	0.4775
Nguyen et al. [70]	MK-TSDT	0.1712	0.2549	0.2949	0.3326	0.3647	0.3949	0.4892
	MK-ESDT	0.1710	0.2546	0.2946	0.3325	0.3646	0.3944	0.4886
	MK-ITSDT	0.1707	0.2542	0.2942	0.3321	0.3641	0.3937	0.4878
Boundary conditions: CCCC								
Present element (4 × 4)	FEM-Q8-LW	0.0751	0.1000	0.1169	0.1368	0.1557	0.1724	0.2158
Present element (6 × 6)	FEM-Q8-LW	0.0750	0.0999	0.1168	0.1366	0.1554	0.1720	0.2153
Present element (8 × 8)	FEM-Q8-LW	0.0750	0.0999	0.1167	0.1366	0.1554	0.1720	0.2153
Gilhooley et al. [71]	HOSNDPT	0.0731	0.1073	0.1253	0.1444	–	–	0.2088
Nguyen et al. [70]	MK-TSDT	0.0713	0.1045	0.1219	0.1404	0.1571	0.1705	0.2036
	MK-ESDT	0.0708	0.1038	0.1212	0.1397	0.1562	0.1692	0.2022
	MK-ITSDT	0.0703	0.1032	0.1205	0.1389	0.1553	0.1680	0.2010

<sup>a</sup>The non-dimensional center deflections are expressed as:  $\bar{w} = \frac{100wE_m h^3}{12(1-\nu^2)q_0 a^4}$

subjected to sinusoidal load,  $q = q_0 \sin(\pi x/a) \sin(\pi y/b)$ . For the current study, five different core-to-face sheets thickness ratio  $h_b-h_c-h_t$  (1-0-1, 2-1-2, 1-1-1, 2-2-1, 1-2-1), three side-to-thickness ratio  $a/h$  (5, 10, 100) and four volume fraction index  $k$  (0, 1, 5, 10) are considered. From the previous example, it is evident that a (6×6) mesh has been found to give good convergence for this type of plates. Therefore, this mesh size is employed in the present analysis. The non-dimensional center deflections are presented in Table 4. The present results are compared with triangular element model (MITC3) of Nguyen et al. [40] using HSDT and those obtained by Pluciński and Jaśkowiec [61] using 3D finite elements models (FEM23-1, ABAQUS). A good agreement between the results is obtained for all schemes, volume fraction index and both thin and thick FGM sandwich plates. Further, it should be noted that the developed element is free from shear locking phenomena where it is able to provide excellent results for thin FGM sandwich plate ( $a/h = 100$ ). Figure 8 show the variation of the non-dimensional deflection with varying volume fraction index ( $k$ ). In addition, the effect of volume fraction index ( $k$ ) on the non-dimensional central deflection for different core-to-face sheets thickness ratio ( $h_c/h_f$ ) is illustrated in Fig. 9. It can be seen that the lowest and highest values of deflection correspond to the (1-0-1) and (1-2-1) FGM sandwich plate, respectively. For the case of (1-2-1) plate, it is observed that as the core

thickness increases, the deflection value decreases. This is due to high proportion of ceramic which leads the plate to be more rigid.

### 5.2 Free vibration analysis

The robustness of the present layerwise finite element formulation is also verified for free vibration analysis of functionally graded sandwich plates.

**Example 3** For the verification purpose, the convergence of developed finite element model is examined for thin and thick square isotropic FGM ( $Al^*/ZrO_2$ ) plate. The plate is simply supported on all four sides. In the present analysis, different side-to-thickness ratio ( $a/h$ ) and volume fraction index ( $k$ ) are considered. The non-dimensional natural frequencies is reported in Table 5 using different mesh sizes ( $4 \times 4$ ,  $6 \times 6$  and  $8 \times 8$ ). The present results are compared with the 3D-elasticity solutions [72], the analytical results based on HSDT [42] as well as finite element solutions [51]. The comparison shows that the performance of the present finite element formulation, for both thin and thick FGM plates, is very good in terms of the efficiency and the rate of convergence with mesh refinement. Indeed, for moderately thick plate ( $a/h = 10$ ), the maximum percentage error predicted by present element in comparison with

**Fig. 7** Effects of volume fraction index ( $k$ ) with different boundary conditions on the non-dimensional center deflexion of  $Al/ZrO_2$  FGM square plate subjected to uniformly distributed load ( $a/h = 5$ )

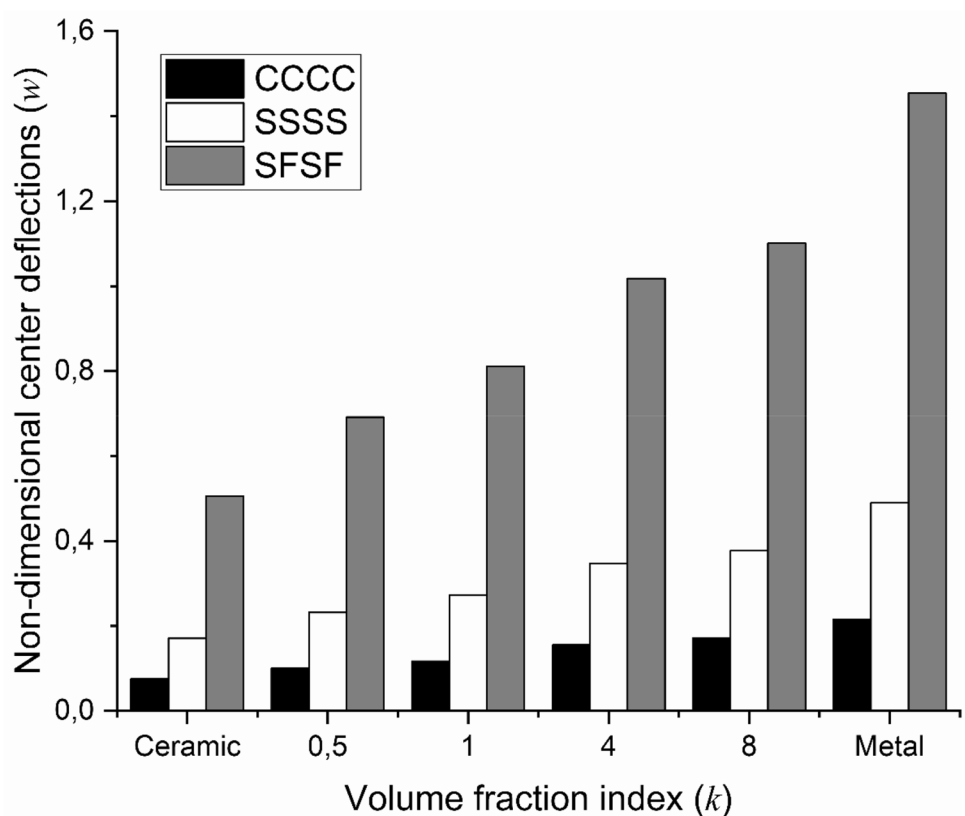


**Table 4** Non-dimensional center deflections ( $\bar{w}$ ) of clamped square sandwich plates with Al/ZrO<sub>2</sub> FGM face sheets subjected to sinusoidally distributed load

<i>a/h</i>	<i>k</i>	Reference	Models	Plate configuration				
				1-0-1	2-1-2	1-1-1	2-2-1	1-2-1
100	0	Present element Nguyen et al. [51] Pluciński and Jaśkowiec [61]	FEM-Q8-LW	0.0944 <sup>a</sup>	0.0944	0.0944	0.0945	0.0944
			MITC3-HSDT	0.0961	0.0961	0.0961	0.0961	0.0961
			FEM23-1	0.0992	0.0992	0.0992	0.0992	0.0992
	1	Present element Nguyen et al. [51] Pluciński and Jaśkowiec [61]	ABAQUS	0.0994	0.0995	0.0995	0.0995	0.0995
			FEM-Q8-LW	0.1561	0.1477	0.1408	0.1355	0.1306
			MITC3-HSDT	0.1601	0.1516	0.1445	0.1389	0.1339
	5	Present element Nguyen et al. [51]	FEM23-1	0.1658	0.1571	0.1497	0.1438	0.1386
			ABAQUS	0.1662	0.1576	0.1501	0.1442	0.1390
			FEM-Q8-LW	0.1978	0.1891	0.1791	0.1686	0.1612
	10	Present element Nguyen et al. [51] Pluciński and Jaśkowiec [61]	MITC3-HSDT	0.2025	0.1945	0.1844	0.1734	0.1661
			FEM-Q8-LW	0.2018	0.1952	0.1859	0.1746	0.1677
			MITC3-HSDT	0.2061	0.2005	0.1915	0.1797	0.1728
10	Present element Nguyen et al. [51] Pluciński and Jaśkowiec [61]	FEM23-1	0.2130	0.2080	0.1988	0.1864	0.1795	
		ABAQUS	0.2135	0.2083	0.1993	0.1869	0.1800	
		FEM-Q8-LW	0.1147	0.1155	0.1161	0.1284	0.1167	
10	0	Present element Nguyen et al. [51] Pluciński and Jaśkowiec [61]	MITC3-HSDT	0.1156	0.1156	0.1156	0.1156	0.1156
			FEM23-1	0.1159	0.1159	0.1159	0.1159	0.1159
			ABAQUS	0.1159	0.1159	0.1159	0.1159	0.1158
	1	Present element Nguyen et al. [51] Pluciński and Jaśkowiec [61]	FEM-Q8-LW	0.1875	0.1777	0.1698	0.1723	0.1585
			MITC3-HSDT	0.1862	0.1760	0.1679	0.1619	0.1563
			FEM23-1	0.1868	0.1766	0.1684	0.1625	0.1567
	5	Present element Nguyen et al. [51]	ABAQUS	0.1868	0.1765	0.1684	0.1625	0.1567
			FEM-Q8-LW	0.2380	0.2266	0.2145	0.2081	0.1939
			MITC3-HSDT	0.2363	0.2238	0.2116	0.1996	0.1909
	10	Present element Nguyen et al. [51] Pluciński and Jaśkowiec [61]	Q8LW	0.2437	0.2340	0.2226	0.2147	0.2013
			MITC3-HSDT	0.2429	0.2312	0.2196	0.2067	0.1983
			FEM23-1	0.2446	0.2337	0.2213	0.2088	0.1993
5	Present element Nguyen et al. [51] Pluciński and Jaśkowiec [61]	ABAQUS	0.2446	0.2334	0.2212	0.2087	0.1992	
		FEM-Q8-LW	0.1568	0.1596	0.1616	0.1919	0.1638	
		MITC3-HSDT	0.1652	0.1652	0.1652	0.1652	0.1652	
1	Present element Nguyen et al. [51] Pluciński and Jaśkowiec [61]	FEM23-1	0.1622	0.1622	0.1622	0.1622	0.1622	
		ABAQUS	0.1622	0.1622	0.1622	0.1622	0.1622	
		FEM-Q8-LW	0.2455	0.2328	0.2238	0.2407	0.2116	
5	Present element Nguyen et al. [51]	MITC3-HSDT	0.2496	0.2351	0.2248	0.2182	0.2111	
		FEM23-1	0.2451	0.2307	0.2205	0.2145	0.2070	
		ABAQUS	0.2451	0.2306	0.2204	0.2144	0.2069	
10	Present element Nguyen et al. [51] Pluciński and Jaśkowiec [61]	FEM-Q8-LW	0.3147	0.2929	0.2758	0.2792	0.2512	
		MITC3-HSDT	0.3195	0.2935	0.2754	0.2619	0.2497	
		FEM-Q8-LW	0.3262	0.3040	0.2860	0.2868	0.2596	
10	Present element Nguyen et al. [51] Pluciński and Jaśkowiec [61]	MITC3-HSDT	0.3346	0.3046	0.2856	0.2709	0.2581	
		FEM23-1	0.3326	0.3054	0.2841	0.2708	0.2546	
		ABAQUS	0.3326	0.3053	0.2839	0.2707	0.2543	

<sup>a</sup>The non-dimensional center deflections are expressed as:  $\bar{w} = 10wh^3E_c/a^4q_0$



**Fig. 8** Variation of the non-dimensional deflection of clamped square 1-0-1 FGM sandwich plate of type C subjected to sinusoidal load for different volume fraction index ( $k$ )

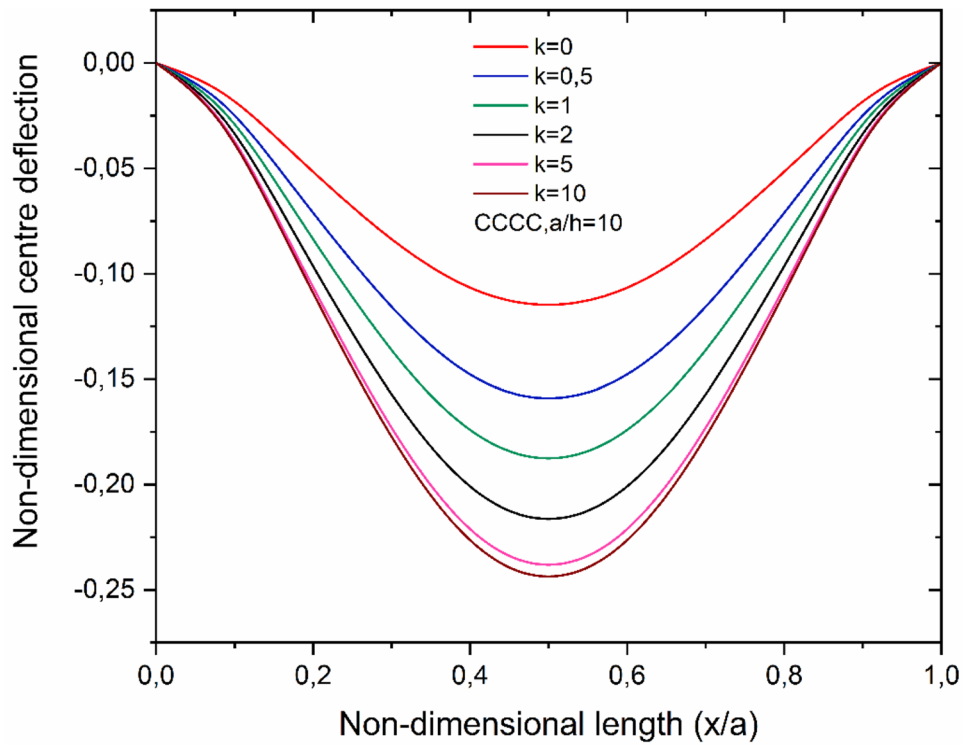


**Fig. 9** Effect of volume fraction index ( $k$ ) with different core-to-face sheets thickness ratio on the non-dimensional center deflection of clamped square sandwich plates with FGM face sheets ( $a/h=10$ )

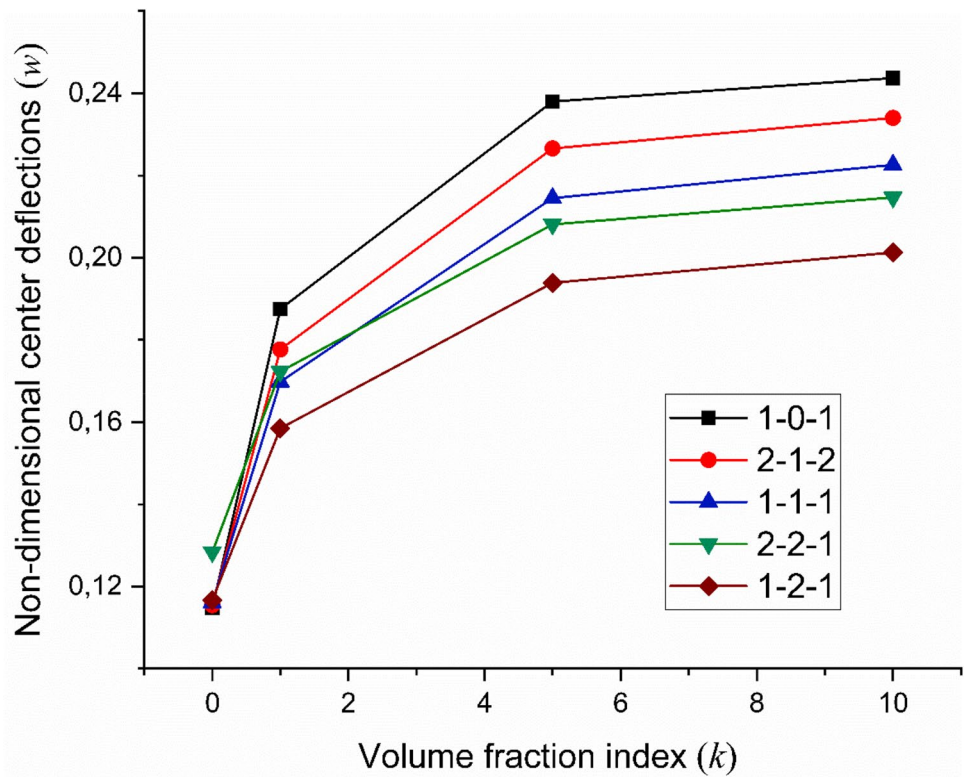


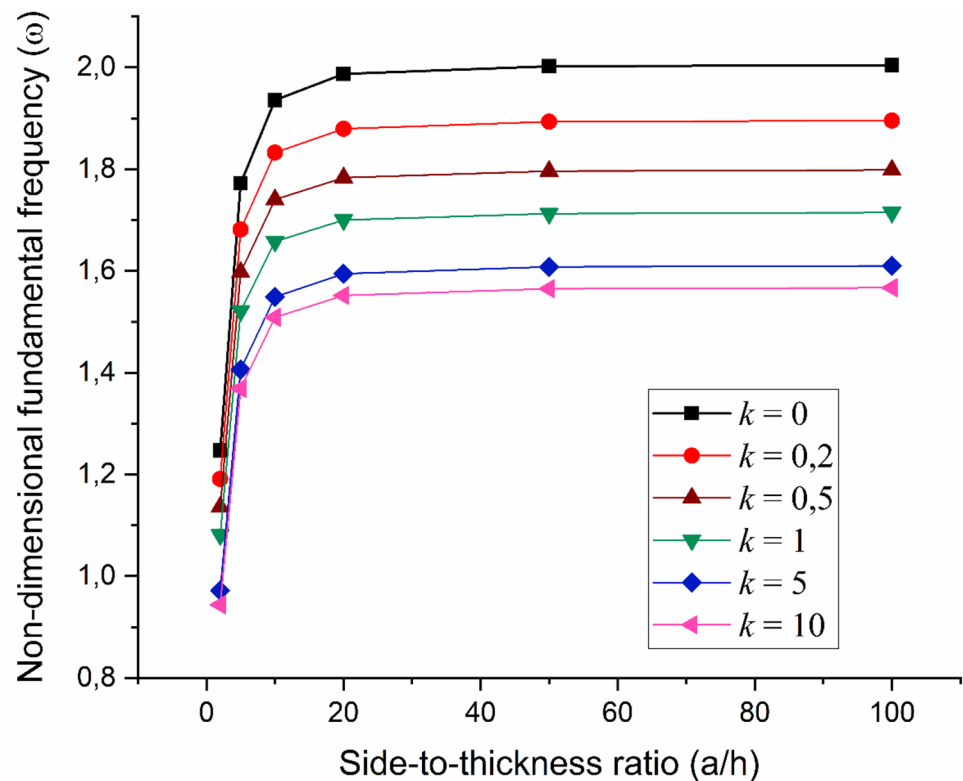
**Table 5** Non-dimensional fundamental frequency ( $\bar{\omega}$ ) of simply supported square Al\*/ZrO<sub>2</sub> FGM plates

a/h	References	Models	k							
			0	0.1	0.2	0.5	1	2	5	10
2	Present element (4×4)	FEM-Q8-LW	1.2476 <sup>b</sup>	1.2160	1.1915	1.1366	1.0816	1.0285	0.9724	0.9449
	Présent element (6×6)	FEM-Q8-LW	1.2470	1.2148	1.1909	1.1360	1.0810	1.0279	0.9718	0.9443
	Présent element (8×8)	FEM-Q8-LW	1.2470	1.2148	1.1909	1.1360	1.0810	1.0279	0.9718	0.9437
	Uymaz and Aydogdu [72]	3D- Elasticity	1.2589	1.2296	1.2049	1.1484	1.0913	1.0344	0.9777	0.9507
	Error <sup>a</sup> (%)		0.9452	1.2036	1,1619	1,0798	0,9438	0,6284	0,6035	0,7363
	Belkhodja et al. [42]	HSDT	1.2538	1.2239	1.1983	1.1412	1.0856	1.0322	0.9748	0.9468
5	Nguyen et al. [51]	MITC3-HSDT	1.2502	1.2210	1.1960	1.1390	1.0821	1.0268	0.9717	0.9466
	Present element (4×4)	FEM-Q8-LW	1.7737	1.7211	1.6830	1.5991	1.5229	1.4618	1.4077	1.3703
	Present element (6×6)	FEM-Q8-LW	1.7725	1.7199	1.6815	1.5979	1.5218	1.4606	1.4065	1.3692
	Present element (8×8)	FEM-Q8-LW	1.7722	1.7196	1.6815	1.5976	1.5214	1.4606	1.4065	1.3692
	Uymaz and Aydogdu [72]	3D- Elasticity	1.7748	1.7262	1.6881	1.6031	1.4764	1.4628	1.4106	1.3711
	Error <sup>a</sup> (%)		0,1465	0,3823	0,3910	0,3431	3,0480	0,1504	0,2907	0,1386
10	Belkhodja et al. [42]	HSDT	1.7687	1.7220	1.6827	1.5979	1.5217	1.4605	1.4059	1.3690
	Nguyen et al. [51]	MITC3-HSDT	1.7782	1.7270	1.6893	1.6057	1.5293	1.4677	1.4132	1.3764
	Present element (4×4)	FEM-Q8-LW	1.9386	1.8774	1.8341	1.7416	1.6595	1.5998	15,505	1.5103
	Present element (6×6)	FEM-Q8-LW	1.9371	1.8759	1.8326	1.7401	1.6580	1.5983	1.5491	1.5088
	Present element (8×8)	FEM-Q8-LW	1.9356	1.8759	1.8326	1.7401	1.6580	1.5983	1.5491	1.5088
	Uymaz and Aydogdu [72]	3D- Elasticity	1.9339	1.8788	1.8357	1.7406	1.6583	1.5968	1.5491	1.5066
20	Error <sup>a</sup> (%)		0,0879	0,1544	0,1689	0,0287	0,0181	0,0939	0,0000	0,1460
	Belkhodja et al. [42]	HSDT	1.9318	1.8785	1.8341	1.7398	1.6583	1.5986	1.5492	1.5083
	Nguyen et al. [51]	MITC3-HSDT	1.9426	1.8863	1.8426	1.7488	1.6674	1.6074	1.5578	1.5168
	Present element (4×4)	FEM-Q8-LW	1.9896	1.9263	1.8816	1.7855	1.7025	1.6434	15,962	1.5544
	Present element (6×6)	FEM-Q8-LW	1.9872	1.9245	1.8798	1.7837	1.7007	1.6416	1.5944	1.5526
	Present element (8×8)	FEM-Q8-LW	1.9872	1.9239	1.8792	1.7831	1.7001	1.6416	1.5944	1.5520
50	Uymaz and Aydogdu [72]	3D- Elasticity	1.9570	1.9261	1.8788	1.7832	1.6999	1.6401	1.5937	1.5491
	Error <sup>a</sup> (%)		1,5432	0,1142	0,0213	0,0056	0,0118	0,0915	0,0439	0,1872
	Belkhodja et al. [42]	HSDT	1.9821	1.9267	1.8806	1.7833	1.7004	1.6415	1.5943	1.5521
	Nguyen et al. [51]	MITC3-HSDT	1.9932	1.9286	1.8822	1.7908	1.7098	1.6507	1.6032	1.5608
	Present element (4×4)	FEM-Q8-LW	2.0080	1.9442	1.8990	1.8016	1.7181	1.6595	1.6125	1.5699
	Present element (6×6)	FEM-Q8-LW	2.0027	1.9389	1.8934	1.7964	1.7132	1.6546	1.6084	1.5655
100	Present element (8×8)	FEM-Q8-LW	2.0020	1.9386	1.8931	1.7960	1.7128	1.6543	1.6080	1.5651
	Uymaz and Aydogdu [72]	3D-Elasticity	1.9974	1.9390	1.8920	1.7944	1.7117	1.6522	1.6062	1.5620
	Error <sup>a</sup> (%)		0,2303	0,0206	0,0581	0,0892	0,0643	0,1271	0,1121	0,1985
	Belkhodja et al. [42]	HSDT	1.9971	1.9410	1.8944	1.7962	1.7129	1.6543	1.6078	1.5652
	Nguyen et al. [51]	MITC3-HSDT	2.0028	1.9274	1.8888	1.8001	1.7188	1.6598	1.6129	1.5700
	Present element (4×4)	FEM-Q8-LW	2.0221	1.9580	1.9236	1.8147	1.7311	1.6714	1.6237	1.5804
100	Present element (6×6)	FEM-Q8-LW	2.0057	1.9416	1.8953	1.7983	1.7162	1.6565	1.6102	1.5685
	Present element (8×8)	FEM-Q8-LW	2.0042	1.9401	1.8953	1.7983	1.7147	1.6565	1.6102	1.5670
	Uymaz and Aydogdu [72]	3D-Elasticity	1.9974	1.9416	1.8920	1.7972	1.7117	1.6552	1.6062	1.5652
	Error <sup>a</sup> (%)		0,3404	0,0773	0,1744	0,0612	0,1753	0,0785	0,2490	0,1150
	Belkhodja et al. [42]	HSDT	1.9993	1.9431	1.8964	1.7981	1.7147	1.6562	1.6098	1.5671
	Nguyen et al. [51]	MITC3-HSDT	2.0050	1.9272	1.8885	1.7999	1.7188	1.6599	1.6132	1.5704

<sup>a</sup>Error = [(Present result- Exact-3D [72] / Exact-3D [72]) × 100

<sup>b</sup>The natural frequencies are expressed as:  $\bar{\omega} = \frac{\omega ab}{\pi^2 h} \sqrt{12(1 - \nu^2) \frac{\rho_c}{E_c}}$

**Fig. 10** Effect of side-to-thickness ratio ( $a/h$ ) with volume fraction index ( $k$ ) on the non-dimensional fundamental frequency of clamped square sandwich plates with FGM face sheets



3D-Exact elasticity solution of Uymaz and Aydogdu [72], is 0.0287%, 0.0181%, 0.0939%, 0.0000% with respect to the volume fraction index ( $k$ ) of 0.5, 1, 2 and 5. For thin plate ( $a/h = 100$ ) with  $k = 0.1$ , the maximum percentage error is about 0.0773% for the present model and 0.7417% for Nguyen model [40] when compared with the exact 3D dimensional solution [72]. Furthermore, the effect of side-to-thickness ratio ( $a/h$ ) and volume fraction index ( $k$ ) on the fundamental natural frequency is illustrated in Fig. 10. It can be seen that the fundamental natural frequency increases with increased side-to-thickness ratio ( $a/h$ ) up to  $a/h = 20$  and then varies constantly in all cases. This probably can be explained by the effect of shear deformation which is less significant when the thickness decreases ( $a/h > 20$ ). To conclude, the non-dimensional fundamental frequency of thick FGM sandwich plates is more sensitive side-to-thickness ratio than that of thin ones. Besides, by increasing the volume fraction index ( $k$ ), the fundamental natural frequency decreases. This is due to the reduction of the rigidity of plate because of the high proportion of metal. This latter having a Young's modulus lower than that of ceramic.

**Example 4** In the 4th example, a rectangular FGM plate made of aluminum (Al) and alumina ( $\text{Al}_2\text{O}_3$ ) is studied for different volume fraction index and side-to-thickness ratio. Both square ( $b = a$ ) and rectangular ( $b = 2a$ ) plates are considered. Numerical results have been obtained for six different combinations of symmetric (SSSS, SCSC, SFSF) and

asymmetric (SCSF, SSSC, SSSF), boundary conditions. Based on the convergence study, a mesh size with  $6 \times 6$  elements is sufficient to obtain an accurate results. The comparison results presented in Table 6 and in Fig. 11 show the accuracy of the developed element where one can see clearly, for all types of boundary conditions, that the present results are in excellent agreement with the 3D-Exact elasticity solutions of Jin et al. [73]. Indeed, for  $b/a = 2$ ,  $a/h = 10$  and  $k = 5$ , the maximum percentage error of fundamental frequency under boundary conditions SSSS, SCSC, SFSF, SCSF, SSSC, and SSSF when compared with the 3D-Exact elasticity solution [73] is 0.2335, 0.5395, 0.0538, 0.1759, 0.3862 and 0.0000, respectively. Further, the excellent accuracy of the new element is insensitive to boundary conditions. In addition, it can be observed, for both square and rectangular FGM plates, that the lowest fundamental natural frequency is observed for SSSF, SFSF and SCSF boundary conditions, while the highest fundamental natural frequency is seen for SCSC and SSSC boundary conditions, as shown in Fig. 11. Generally speaking, the natural frequencies increase as the rigidity of boundary restraint is increased.

**Example 5** After establishing the performance of present model for isotropic FGM plates, the free vibration analysis of square sandwich plates with FGM face sheets and homogenous core (Type C) is examined in this example. The plate is simply supported on all four sides. The present study is performed for two cases of FGM sandwich plates,

**Table 6** Non-dimensional fundamental frequency ( $\bar{\omega}$ ) of rectangular Al/Al<sub>2</sub>O<sub>3</sub> FGM plates with different boundary conditions

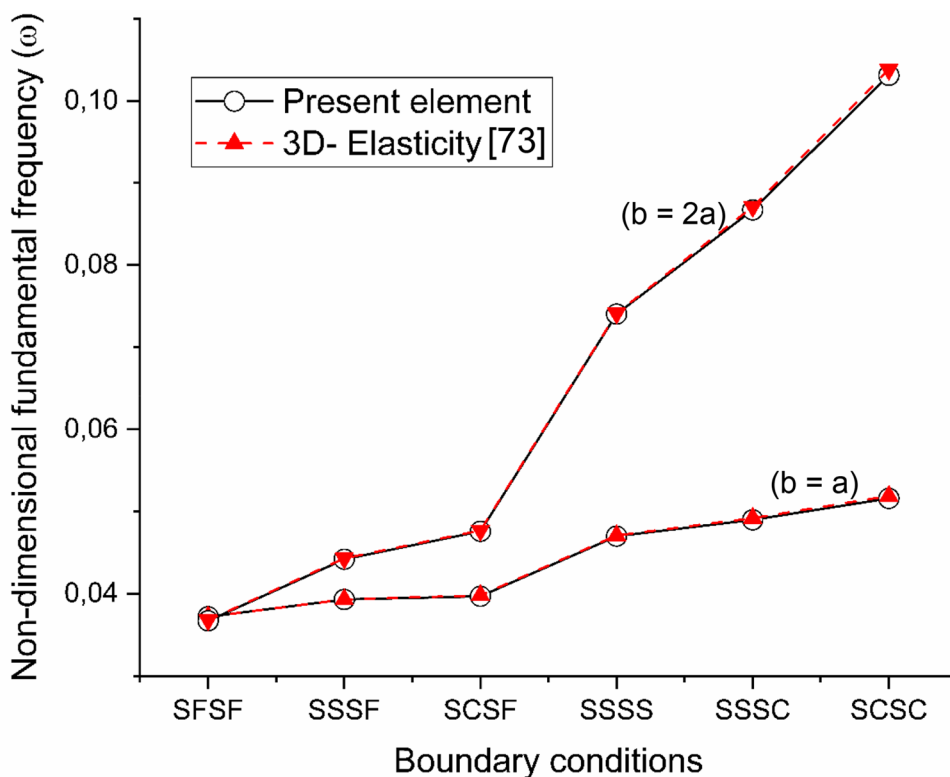
<i>b/a</i>	<i>a/h</i>	<i>k</i>	Reference	Models	BCs					
					SSSS	SCSC	SFSF	SCSF	SSSC	SSSF
1	10	0	Present element	FEM-Q8-LW	0.1137 <sup>a</sup>	0.1592	0.0563	0.0731	0.1336	0.0678
			Jin et al. [73]	3D-Elasticity	0.1135	0.1604	0.0562	0.0731	0.1339	0.0677
		1	Present element	FEM-Q8-LW	0.0868	0.1225	0.0429	0.0557	0.1023	0.0517
			Jin et al. [73]	3D-Elasticity	0.0870	0.1236	0.0430	0.0559	0.1029	0.0518
		2	Present element	FEM-Q8-LW	0.0787	0.1109	0.0389	0.0506	0.0927	0.0469
			Jin et al. [73]	3D-Elasticity	0.0789	0.1118	0.0390	0.0507	0.0932	0.0470
	5	Present element	FEM-Q8-LW	0.0740	0.1031	0.0367	0.0476	0.0867	0.0442	
		Jin et al. [73]	3D-Elasticity	0.0741	0.1038	0.0368	0.0477	0.0871	0.0443	
	5	0	Present element	FEM-Q8-LW	0.4163	0.5351	0.2144	0.2712	0.4707	0.2553
			Jin et al. [73]	3D-Elasticity	0.4169	0.5402	0.2141	0.2713	0.4731	0.2550
		1	Present element	FEM-Q8-LW	0.3207	0.4204	0.1642	0.2085	0.3658	0.1957
			Jin et al. [73]	3D-Elasticity	0.3222	0.4236	0.1645	0.2092	0.3681	0.1962
		2	Present element	FEM-Q8-LW	0.2895	0.3793	0.1486	0.1884	0.3300	0.1770
			Jin et al. [73]	3D-Elasticity	0.2905	0.3799	0.1488	0.1889	0.3310	0.1773
		5	Present element	FEM-Q8-LW	0.2673	0.3445	0.1386	0.1748	0.3023	0.1647
Jin et al. [73]			3D-Elasticity	0.2676	0.3412	0.1388	0.1749	0.3014	0.1649	
2		10	0	Present element	FEM-Q8-LW	0.0707	0.0792	0.0584	0.0608	0.0751
	Jin et al. [73]			3D-Elasticity	0.0719	0.0793	0.0568	0.0607	0.0751	0.0600
	1		Present element	FEM-Q8-LW	0.0548	0.0604	0.0434	0.0463	0.0573	0.0458
			Jin et al. [73]	3D-Elasticity	0.0550	0.0608	0.0435	0.0465	0.0575	0.0459
	2		Present element	FEM-Q8-LW	0.0498	0.0548	0.0394	0.0421	0.0520	0.0416
			Jin et al. [73]	3D-Elasticity	0.0499	0.0552	0.0395	0.0422	0.0522	0.0417
	5	Present element	FEM-Q8-LW	0.0469	0.0516	0.0372	0.0397	0.0490	0.0393	
		Jin et al. [73]	3D-Elasticity	0.0471	0.0519	0.0372	0.0398	0.0492	0.0393	
	5	0	Present element	FEM-Q8-LW	0.2713	0.2931	0.2169	0.2304	0.2810	0.2284
			Jin et al. [73]	3D-Elasticity	0.2713	0.2941	0.2166	0.1914	0.2814	0.1914
		1	Present element	FEM-Q8-LW	0.2081	0.2257	0.1661	0.1767	0.2159	0.1750
			Jin et al. [73]	3D-Elasticity	0.2088	0.2271	0.1665	0.1592	0.2169	0.1592
		2	Present element	FEM-Q8-LW	0.1883	0.20396	0.1504	0.1599	0.1952	0.1584
			Jin et al. [73]	3D-Elasticity	0.1888	0.2050	0.1507	0.1438	0.1960	0.1438
		5	Present element	FEM-Q8-LW	0.1753	0.1888	0.1405	0.1492	0.1814	0.1479
Jin et al. [73]			3D-Elasticity	0.1754	0.1895	0.1405	0.1243	0.1817	0.1243	

<sup>a</sup>The natural frequencies are expressed as:  $\bar{\omega} = \omega h \sqrt{\rho_m / E_m}$

namely, hardcore and softcore. In the case of hardcore, the bottom face sheet is graded from ceramic to metal (Al<sub>2</sub>O<sub>3</sub>/Al) and the core layer is made of pure metal (Al). For the case of softcore, the plate is made of pure ceramic core (Al<sub>2</sub>O<sub>3</sub>) and the upper and lower surfaces of the bottom face sheet are rich in metal and ceramic (Al/Al<sub>2</sub>O<sub>3</sub>), respectively. The computed results are obtained for five different core-to-face sheets thickness ratio  $h_b-h_c-h_t$  (1-0-1, 2-1-2, 1-1-1, 1-2-1, 1-8-1), three side-to-thickness ratio  $a/h$  (5, 10, 100) and five volume fraction index  $k$  (0, 0.5, 1, 5, 10). A mesh size of  $6 \times 6$  is considered for the analysis. The accuracy of the developed finite element, for both hardcore and softcore, can be seen, respectively, in Table 7 and 8. One can see clearly that the present results are very close to those

of 3D-elasticity solutions of Li, Iu et al. [3], the finite element model of Pandey and Pradyumna [37] and the meshless solution based on spline radial basis function by Xiang et al. [74]. It can be clearly seen, from these results, that the non-dimensional fundamental frequencies for hardcore FGM sandwich plates decreased with an increase in volume fraction index (see Fig. 12), whereas the opposite nature of variation in non-dimensional fundamental frequencies is observed for softcore FGM sandwich plates (see Fig. 13). This is due to the difference in stiffness parameters due to change in material properties. It is also pointed out that, for hardcore FGM sandwich plates, the non-dimensional fundamental frequencies is maximum for (1-8-1) plate and minimum for (1-0-1) plate, whereas for softcore FGM

**Fig. 11** Effect of aspect ratio ( $b/a$ ) with different boundary conditions on the non-dimensional fundamental frequency of Al/Al<sub>2</sub>O<sub>3</sub> FGM plate ( $a/h = 10$ ,  $k = 5$ )



sandwich plates, the non-dimensional fundamental frequencies reaches its maximum for (1-0-1) plate and minimum for (1-8-1) plate.

**Example 6** To check the higher order modes of vibration, a square FGM sandwich plate of type C is investigated with  $h_r-h_c-h_b = 2-1-2$ . The bottom face sheet is graded from metal to ceramic (Al/Al<sub>2</sub>O<sub>3</sub>) and the core is made a fully ceramic material (Al<sub>2</sub>O<sub>3</sub>). Two different boundary conditions (SSSS and CCCC) with two side-to-thickness ratio ( $a/h = 10$  and 100) and volume fraction index ( $k = 1$  and 10) are considered in the present study. The non-dimensional natural frequencies of the first-five mode shapes are shown in Table 9. Based on the convergence study, a mesh size with  $8 \times 8$  elements is sufficient to obtain good results. The obtained results are compared with the 3D-elasticity solutions [3] and various numerical results found in the literature, such as, the eight nodes quadrilateral finite element model based on HSDT [50], the meshfree solution based on TSDT [70] and the isogeometric results (IGA) based on four-unknown shear and normal deformations theory (SNDT) [22]. It is evident from the results of comparison that the proposed finite element model agree very well with both the 3D-elasticity solutions [52] and the numerical models available in the literature. Further, the developed element is free from transverse shear locking, and its excellent accuracy is insensitive to thin FGM sandwich plates. The first six flexural mode shapes

of a simply supported FGM sandwich plates of type C, are plotted in Fig. 14 for  $a/h = 10$  and  $k = 1$ .

**Example 7** After studying the free vibration of sandwich plate with FGM face sheets, a simply supported square sandwich plate with FGM core and homogenous face sheets (Type B) is analyzed with  $h_r-h_c-h_b = 1-8-1$  ( $h_2 = 0.8 h$  and  $h_1 = h_3 = 0.1$ ). The top and bottom face sheets are made of pure metal (Al) and ceramic (Al<sub>2</sub>O<sub>3</sub>), respectively, whereas the FGM core layer is graded from ceramic to metal (Al<sub>2</sub>O<sub>3</sub>/Al). Three values of side-to-thickness ratio ( $a/h = 5, 10, 100$ ) with five different volume fraction index ( $k = 0.5, 1, 2, 5, 10$ ) are considered for the investigation. The non-dimensional fundamental frequencies predicted by the present layerwise model are listed in Table 10 with different mesh size ( $4 \times 4, 6 \times 6$  and  $8 \times 8$ ). For comparison purposes, 3D-elasticity solutions derived by Li et al. [3], hyperbolic higher order shear deformation theory (HHSDT) computed by Bennoun, Houari et al. [39], semi analytical solutions based on differential quadrature method (DQM) given by Alibeigloo and Alizadeh [75] as well as those obtained by Pandey and Pradyumna [46] using layerwise finite element solutions, are carried out. According the Table 9, it can be observed that the obtained result, for all cases presented, are in excellent agreement with reported literature values and even more accurate than those predicted by the analytical solutions of Bennoun, Houari et al. [39] using HHSDT. For example,

**Table 7** Non-dimensional fundamental frequency ( $\bar{\omega}$ ) of simply supported square FGM sandwich plates with homogeneous hardcore

$a/h$	$k$	References	Models	Plate configuration					
				1-0-1	2-1-2	1-1-1	1-2-1	1-8-1	
100	0	Present element Li et al. [3]	FEM-Q8-LW	1.8890 <sup>a</sup>	1.8890	1.8890	1.8890	1.8890	
			3D-Elasticity	1.8882	1.8882	1.8882	1.8882	1.8882	
	0.5	Present element Li et al. [3]	FEM-Q8-LW	1.4840	1.5240	1.5610	1.6200	1.7640	
			3D-Elasticity	1.4824	1.5235	1.5604	1.6191	1.7635	
	1	Present element Li et al. [3]	FEM-Q8-LW	1.2740	1.3310	1.3860	1.4760	1.7000	
			3D-Elasticity	1.2715	1.3297	1.3851	1.4755	1.6990	
	5	Present element Li et al. [3]	FEM-Q8-LW	0.9650	0.9998	1.0640	1.1980	1.5710	
			3D-Elasticity	0.9656	0.9990	1.0630	1.1969	1.5698	
	10	Present element Li et al. [3]	FEM-Q8-LW	0.9503	0.9601	1.0130	1.1450	1.5430	
			3D-Elasticity	0.9504	0.9593	1.0123	1.1440	1.5416	
	10	0	Present element Li et al. [3]	FEM-Q8-LW	1.8330	1.8300	1.8290	1.8270	1.8250
				3D-Elasticity	1.8268	1.8268	1.8268	1.8268	1.8268
0.5		Present element Li et al. [3]	FEM-Q8-LW	1.4480	1.4860	1.5210	1.5750	1.7090	
			3D-Elasticity	1.4461	1.4860	1.5213	1.5766	1.7113	
1		Present element Li et al. [3]	FEM-Q8-LW	1.2460	1.3010	1.3540	1.4400	1.6490	
			3D-Elasticity	1.2447	1.3018	1.3552	1.4413	1.6511	
5		Present element Li et al. [3]	FEM-Q8-LW	0.9458	0.9808	1.0440	1.1740	1.5280	
			3D-Elasticity	0.9447	0.9810	1.0453	1.1756	1.5299	
10		Present element Li et al. [3]	FEM-Q8-LW	0.9276	0.9410	0.9945	1.1230	1.5010	
			3D-Elasticity	0.9272	0.9407	0.9952	1.1246	1.5033	
5		0	Present element Li et al. [3]	FEM-Q8-LW	1.6937	1.6872	1.6822	1.6760	1.6710
				3D-Elasticity	1.6771	1.6771	1.6771	1.6771	1.6771
	0.5	Present element Li et al. [3]	FEM-Q8-LW	1.3565	1.3900	1.4195	1.4650	1.5750	
			3D-Elasticity	1.3535	1.3905	1.4217	1.4694	1.5810	
	1	Present element Li et al. [3]	FEM-Q8-LW	1.1747	1.2260	1.2735	1.3480	1.5245	
			3D-Elasticity	1.1748	1.2291	1.2777	1.3534	1.5314	
	5	Present element Li et al. [3]	FEM-Q8-LW	0.8930	0.9320	0.9935	1.1125	1.4212	
			3D-Elasticity	0.8908	0.9336	0.9979	1.1190	1.4284	
	10	Present element Li et al. [3]	FEM-Q8-LW	0.8707	0.8925	0.9465	1.0662	1.3985	
			3D-Elasticity	0.8683	0.8922	0.9498	1.0729	1.4056	

<sup>a</sup>The natural frequencies are expressed as:  $\bar{\omega} = \omega b^2 / h \sqrt{\rho_0 / E_0}$

with  $a/h = 100$ , the maximum error predicted by present model, when compared with exact 3D-elasticity solutions [3], is only 0.0223%, 0.0288%, 0.0069%, 0.0391%, 0.0000%, with respect to the volume fraction index ( $k$ ) of 0.5, 1, 2, 5,10, whereas the maximum error of the HHSdT model [39] is 2.3146%, 2.1779%, 1.6956%, 0.9599%, 0.5971%. As expected, the comparison confirms the high accuracy of the developed layerwise model. It can be concluded that the proposed finite element formulation is not only accurate but also simple in predicting the natural frequencies of FGM sandwich plates. Moreover, it can be clear from Table 10 that the fundamental natural frequency of FGM sandwich

plate of type B increase when the values of volume fraction index ( $k$ ) changes from 0.5 to 10.

### 6 Conclusion

In the current study, for the first time, the original layer-wise formulation has been generalized to predict accurately the deflection and natural frequency of functionally graded sandwich plates. The proposed model assumes a first-order shear deformation theory in the face sheets and a higher-order displacement field in the core maintaining a continuity

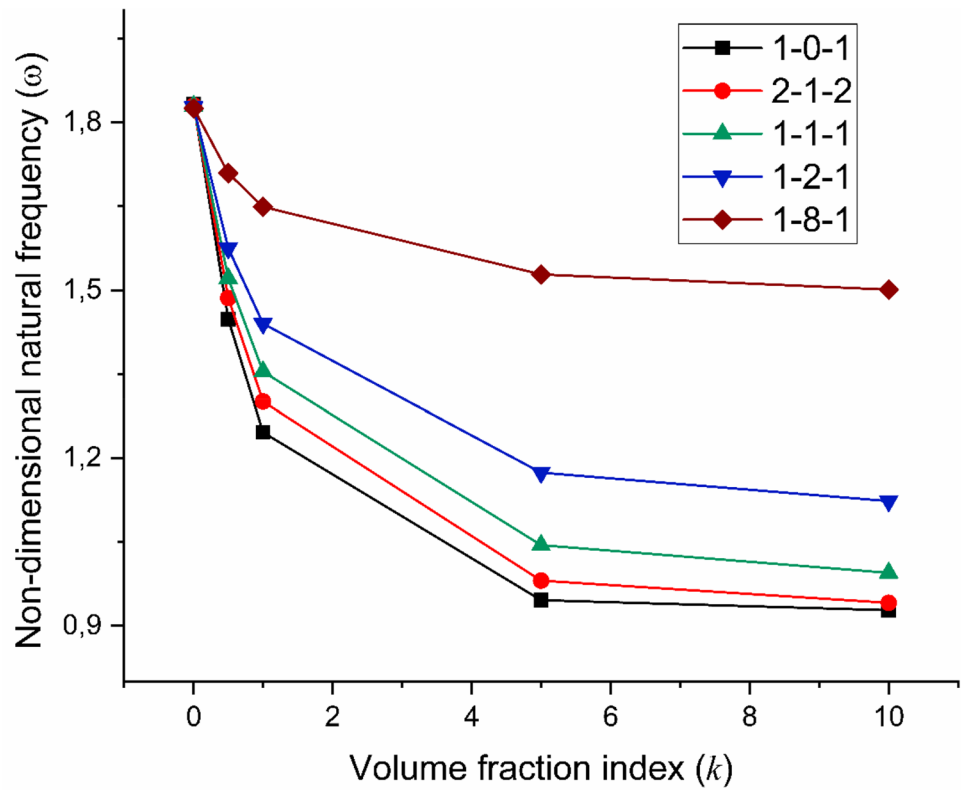
**Table 8** Non-dimensional fundamental frequency ( $\bar{\omega}$ ) of simply supported square FGM sandwich plates with homogeneous softcore

$a/h$	$k$	References	Models	Plate configuration					
				1-0-1	2-1-2	1-1-1	1-2-1	1-8-1	
100	0	Present element	FEM-Q8-LW	0.9607	0.9607	0.9607	0.9607	0.9607	
		Li et al. [3]	3D-Elasticity	0.9602	0.9602	0.9602	0.9602	0.9602	
	0.5	Present element	FEM-Q8-LW	1.6630	1.6240	1.5830	1.5070	1.2660	
		Li et al. [3]	3D-Elasticity	1.6628	1.6229	1.5817	1.5065	1.2655	
		Pandey and Pradyumna [46]	Q8-LW	–	1.6317	1.5826	1.5073	1.2661	
	1	Present element	FEM-Q8-LW	1.8210	1.7930	1.7550	1.6760	1.3840	
		Li et al. [3]	3D-Elasticity	1.8203	1.7916	1.7537	1.6749	1.3833	
		Pandey and Pradyumna [46]	Q8-LW	–	1.7926	1.7547	1.6756	1.3839	
	5	Present element	FEM-Q8-LW	1.9240	1.9440	1.9370	1.8860	1.5710	
		Li et al. [3]	3D-Elasticity	1.9209	1.9431	1.9362	1.8853	1.5703	
		Pandey and Pradyumna [46]	Q8-LW	–	1.9439	1.9370	1.8860	1.5709	
	10	Present element	FEM-Q8-LW	1.9140	1.9470	1.9510	1.9120	1.6050	
		Li et al. [3]	3D-Elasticity	1.9106	1.9468	1.9504	1.9116	1.6045	
		Pandey and Pradyumna [46]	Q8-LW	–	1.9475	1.9511	1.9123	1.6052	
	10	0	Present element	FEM-Q8-LW	0.9319	0.9308	0.9300	0.9290	0.9280
			Li, et al. [3]	3D-Elasticity	0.9289	0.9289	0.9289	0.9289	0.9289
0.5		Present element	FEM-Q8-LW	1.5980	1.5430	1.4960	1.4220	1.2050	
		Li et al. [3]	3D-Elasticity	1.5735	1.5258	1.4845	1.4166	1.2055	
		Pandey and Pradyumna [46]	Q8-LW	–	1.5430	1.4960	1.4217	1.2060	
1		Present element	FEM-Q8-LW	1.7500	1.6920	1.6430	1.5630	1.3080	
		Li et al. [3]	3D-Elasticity	1.7222	1.6743	1.6305	1.5578	1.3082	
		Pandey and Pradyumna [46]	Q8-LW	–	1.6927	1.6435	1.5636	1.3086	
		Xiang et al. [74]		–	1.7060	1.6647	–	1.3115	
5		Present element	FEM-Q8-LW	1.8560	1.8170	1.7850	1.7250	1.4640	
		Li et al. [3]	3D-Elasticity	1.8419	1.8261	1.7895	1.7267	1.4664	
		Pandey and Pradyumna [46]	Q8-LW	–	1.8178	1.7853	1.7250	1.4643	
		Xiang et al. [74]		–	1.8617	1.8469	–	1.4771	
10		Present element	FEM-Q8-LW	1.8490	1.8180	1.7930	1.7420	1.4910	
		Li et al. [3]	3D-Elasticity	1.8402	1.8398	1.8081	1.7481	1.4948	
		Pandey and Pradyumna [46]	Q8-LW	–	1.8284	1.7928	1.7418	1.4915	
5		0	Present element	FEM-Q8-LW	0.8612	0.8580	0.8555	0.8525	0.8497
	Li et al. [3]		3D-Elasticity	0.8528	0.8528	0.8528	0.8528	0.8528	
	0.5	Present element	FEM-Q8-LW	1.4465	1.3637	1.3092	1.2387	1.0690	
		Li et al. [3]	3D-Elasticity	1.3789	1.3206	1.2805	1.2258	1.0701	
	1	Present element	FEM-Q8-LW	1.5850	1.4772	1.4127	1.3345	1.1430	
		Li et al. [3]	3D-Elasticity	1.5089	1.4332	1.3824	1.3212	1.1445	
	5	Present element	FEM-Q8-LW	1.6952	1.5592	1.4927	1.4225	1.2450	
		Li et al. [3]	3D-Elasticity	1.6586	1.5801	1.5028	1.4266	1.2521	
	10	Present element	FEM-Q8-LW	1.6940	1.5565	1.4922	1.4270	1.2607	
		Li et al. [3]	3D-Elasticity	1.6727	1.6090	1.5267	1.4410	1.2706	

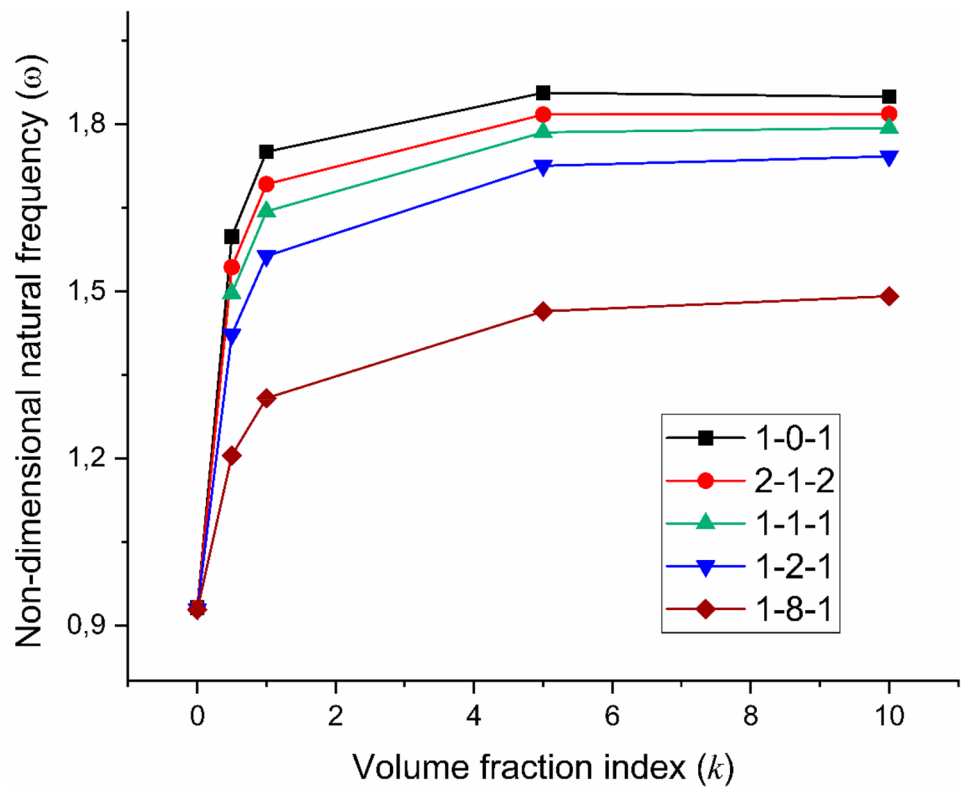
of displacement at layer. Three common types of FGM plates have been taken into consideration: (i) isotropic FGM plates; (ii) sandwich plates with FGM face sheets and homogeneous core and (iii) sandwich plates with homogeneous face sheets and FGM core. Based on the suggested model,

an improved  $C^0$  eight-node quadrilateral element has been successfully developed. Several numerical examples have been performed to assess the performance and reliability of the developed layerwise finite element model. The obtained results have been compared with 3D, quasi-3D, and 2D

**Fig. 12** Effect of volume fraction index ( $k$ ) with different core-to-face sheets thickness ratio on the non-dimensional fundamental frequency of hardcore FGM sandwich plates ( $alh=10$ )



**Fig. 13** Effect of volume fraction index ( $k$ ) with different core-to-face sheets thickness ratio on the non-dimensional fundamental frequency of softcore FGM sandwich plates ( $alh=10$ )





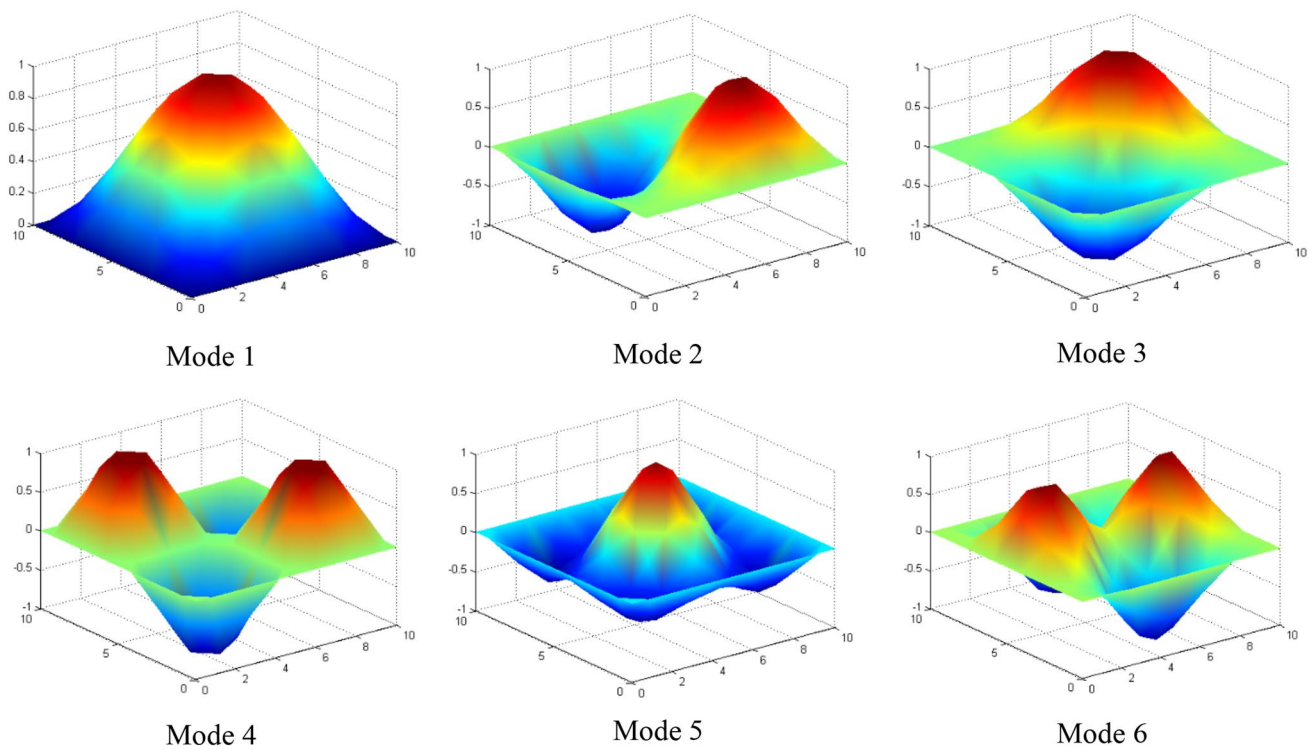


**Fig. 14** First six flexural mode shapes of a simply supported FGM sandwich plates of type C. ( $alh = 10$  and  $k = 1$ )

analytical solutions and those predicted by advanced finite element models available in the literature. The comparison showed that the result accuracy, fast rate of convergence and broad range of applicability of the proposed finite element model, for both thin and thick FGM isotropic and sandwich plates, are excellent. Furthermore, the effects of volume fraction index, material distribution, side-to-thickness ratio, aspect ratios, core-to-face thickness ratio, type of core (hard/soft), frequency modes, and boundary conditions on the natural frequency have been all investigated and reported. From the numerical illustration, the key points of the present study are the following:

- The combination between both equivalent single layer approach and layerwise approach is very advantageous, because the result of present model combines the features of both approaches, which are the simplicity and the accuracy. Thus, the plate theory enjoys the advantage of a single-layer plate theory, even though it is based on the concept of a layerwise plate approach.
- From a computational cost point of view, it is important to mention here that the proposed layerwise finite element formulation needs only  $C^0$  shape functions that contributes to a noticeable decrease of computational efforts.
- The developed finite element is free of shear locking phenomenon without requiring any shear correction factors.
- The non-dimensional deflection increases with the increase of the volume fraction index ( $k$ ).
- The natural frequency increases with the increase of side-to-thickness ratio ( $alh$ ) up to  $alh \leq 20$  while further increasing this ratio ( $alh > 20$ ) has no remarkable effect on the natural frequency.
- The natural frequency of thick FGM sandwich plates is more sensitive side-to-thickness ratio ( $alh$ ) than that of thin ones.
- For all types of boundary conditions, the natural frequency decreases by increasing the volume fraction index ( $k$ ) and the plate's aspect ratio ( $b/a$ ).
- The lowest natural frequency is observed for SSSF, SFSF and SCSF boundary conditions, while the highest fundamental natural frequency is seen for SCSC

**Table 9** First five non-dimensional fundamental frequency ( $\bar{\omega}$ ) of square 2-1-2 FGM sandwich plates (Al/Al<sub>2</sub>O<sub>3</sub>) of type C with two different boundary conditions

<i>a/h</i>	<i>k</i>	References	Models	Modes					
				1	2	3	4	5	
Boundary conditions: SSSS									
10	1	Present element (4×4)	FEM-Q8-LW	1.3020	3.1930	3.1930	5.0320	6.3830	
		Present element (6×6)	FEM-Q8-LW	1.3010	3.1610	3.1610	4.9190	6.0950	
		Present element (8×8)	FEM-Q8-LW	1.3010	3.1550	3.1550	4.9080	6.0450	
		Li et al. [3]	3D-Elasticity	1.3018	3.1587	3.1587	4.9165	6.0404	
		Thai et al. [22]	IGA-SNDT	1.3128	3.1992	3.1992	4.9874	6.1306	
	Natarajan and Manickam [50]	FEM-Q8-HSDT	1.3019	3.1606	3.1606	4.9188	6.0586		
	Nguyen et al. [70]	MK-TSDT	1.3016	3.1484	3.1484	4.9141	5.3609		
	10	10	Present element (8×8)	FEM-Q8-LW	0.9409	2.2900	2.2900	3.5720	4.4080
			Li et al. [3]	3D-Elasticity	0.9404	2.2861	2.2861	3.5646	4.3844
			Thai et al. [22]	IGA-SNDT	0.9625	2.3695	2.3695	3.7192	4.3937
Natarajan and Manickam [50]			FEM-Q8-HSDT	0.9418	2.2948	2.2948	3.5832	4.4225	
Nguyen et al. [70]			MK-TSDT	0.9441	2.2997	2.2997	3.6119	4.3984	
100	1	Present element (8×8)	FEM-Q8-LW	1.3300	3.3270	3.3270	5.3370	6.6770	
		Li et al. [3]	3D-Elasticity	1.3297	3.3232	3.3232	5.3154	6.6428	
	10	Present element (8×8)	FEM-Q8-LW	0.9595	2.4010	2.4010	3.8550	4.8190	
		Li et al. [3]	3D-Elasticity	0.9593	2.3976	2.3976	3.8350	4.7928	
Boundary conditions: CCCC									
10	1	Present element (4×4)	FEM-Q8-LW	2.2980	4.5830	4.5830	6.6550	8.2170	
		Present element (6×6)	FEM-Q8-LW	2.2810	4.4680	4.4680	6.3600	7.6650	
		Present element (8×8)	FEM-Q8-LW	2.2790	4.4510	4.4510	6.3270	7.5640	
		Li et al. [3]	3D-Elasticity	2.2904	4.4672	4.4672	6.3505	7.5600	
		10	Present element (8×8)	FEM-Q8-LW	1.6590	3.2570	3.2570	4.6480	5.5710
	Li et al. [3]	3D-Elasticity	1.6607	3.2493	3.2493	4.6307	5.5217		
	100	1	Present element (8×8)	FEM-Q8-LW	2.4430	5.0230	5.0230	7.6410	9.0630
			Li et al. [3]	3D-Elasticity	2.4334	4.9581	4.9581	7.3059	8.8860
		10	Present element (8×8)	FEM-Q8-LW	1.7670	3.6390	3.6390	5.5790	6.5680
			Li et al. [3]	3D-Elasticity	1.7557	3.5774	3.5774	5.2717	6.4120

and SSSC boundary conditions. Hence, the natural frequency increases as the rigidity of boundary restraint is increased.

- The natural frequency for hardcore FGM sandwich plates decreased with an increase in volume fraction index (*k*), whereas the opposite nature of variation in natural frequency is observed for softcore FGM sandwich plates.
- For hardcore FGM sandwich plates, the natural frequency is maximum for (1-8-1) plate and minimum for (1-0-1) plate, whereas for softcore FGM sandwich plates, the

natural frequency reaches its maximum for (1-0-1) plate and minimum for (1-8-1) plate.

- In the case of sandwich plate with FGM core, the natural frequency increases when the values of volume fraction index (*k*) changes from 0.5 to 10.

It is concluded that the present layerwise finite element model is not only accurate, but also simple in solving the free vibration problems for all types of FGM sandwich plates.

**Table 10** Non-dimensional natural frequency ( $\bar{\omega}$ ) of simply supported sandwich plate 1-8-1 with FGM core (Type B,  $Al_2O_3/Al$ )

$a/h$	References	Models	$k$				
			0.5	1	2	5	10
100	Present element (4×4)	FEM-Q8-LW	1.3540	1.4030	1.4620	1.5490	1.6090
	Présent element (6×6)	FEM-Q8-LW	1.3400	1.3870	1.4460	1.5320	1.5920
	Présent element (8×8)	FEM-Q8-LW	1.3390	1.3870	1.4450	1.5320	1.5910
	Li et al. [3]	3D-Elasticity	1.3393	1.3866	1.4449	1.5314	1.5910
	Pandey and Pradyumna [46]	Q8-LW	1.3400	1.3874	–	1.5318	1.5914
	Bennoun et al. [33]	HHSDT	1.3703	1.4168	1.4694	1.5461	1.6005
	Alibeigloo and Alizadeh [75]	DQM	1.3392	1.3876	1.4465	1.5341	1.5949
10	Present element (4×4)	FEM-Q8-LW	1.2900	1.3430	1.4040	1.4900	1.5470
	Present element (6×6)	FEM-Q8-LW	1.2890	1.3410	1.4020	1.4890	1.5460
	Present element (8×8)	FEM-Q8-LW	1.2890	1.3410	1.4020	1.4880	1.5460
	Li et al. [3]	3D-Elasticity	1.2975	1.3484	1.4082	1.4930	1.5498
	Pandey and Pradyumna [46]	Q8-LW	1.2981	1.3482	–	1.4922	1.5497
	Bennoun et al. [39]	HHSDT	1.3263	1.3765	1.4312	1.5070	1.5591
	Alibeigloo and Alizadeh [75]	DQM	1.2976	1.3494	1.4097	1.4956	1.5949
5	Present element (4×4)	FEM-Q8-LW	1.1717	1.2322	1.2972	1.3817	1.4340
	Present element (6×6)	FEM-Q8-LW	1.1710	1.2312	1.2962	1.3805	1.4330
	Present element (8×8)	FEM-Q8-LW	1.1707	1.2312	1.2960	1.3805	1.4327
	Li et al. [3]	3D-Elasticity	1.1958	1.2533	1.3156	1.3956	1.4454
	Alibeigloo and Alizadeh [75]	DQM	1.1963	1.2547	1.3173	1.3980	1.4492

## References

- Vinson JR (2001) Sandwich structures. *Appl Mech Rev* 54(3):201–214
- Wang Z-X, Shen H-S (2012) Nonlinear vibration and bending of sandwich plates with nanotube-reinforced composite face sheets. *Compos B Eng* 43(2):411–421
- Li Q, Iu V, Kou K (2008) Three-dimensional vibration analysis of functionally graded material sandwich plates. *J Sound Vib* 311(1–2):498–515
- Sofiyev A, Osmancebioglu E (2017) The free vibration of sandwich truncated conical shells containing functionally graded layers within the shear deformation theory. *Compos B Eng* 120:197–211
- Anderson TA (2003) A 3-D elasticity solution for a sandwich composite with functionally graded core subjected to transverse loading by a rigid sphere. *Compos Struct* 60(3):265–274
- Vel SS, Batra R (2004) Three-dimensional exact solution for the vibration of functionally graded rectangular plates. *J Sound Vib* 272(3–5):703–730
- Kashtalyan M, Menshykova M (2009) Three-dimensional elasticity solution for sandwich panels with a functionally graded core. *Compos Struct* 87(1):36–43
- Swaminathan K, Naveenkumar D, Zenkour A et al (2015) Stress, vibration and buckling analyses of FGM plates. A state-of-the-art review. *Compos Struct* 120:10–31
- Ebrahimi MJ, Najafizadeh MM (2014) Free vibration analysis of two-dimensional functionally graded cylindrical shells. *Appl Math Model* 38(1):308–324
- Chi S-H, Chung Y-L (2006) Mechanical behavior of functionally graded material plates under transverse load. Part I: Analysis. *Int J Solids Struct* 43(13):3657–3674
- Zhang D-G, Zhou Y-H (2008) A theoretical analysis of FGM thin plates based on physical neutral surface. *Comput Mater Sci* 44(2):716–720
- Abrate S (2008) Functionally graded plates behave like homogeneous plates. *Compos B Eng* 39(1):151–158
- Avcar M, Mohammed WKM (2018) Free vibration of functionally graded beams resting on Winkler-Pasternak foundation. *Arab J Geosci* 11(10):232
- Civalek Ö, Uzun B, Yaylı MÖ et al (2020) Size-dependent transverse and longitudinal vibrations of embedded carbon and silica carbide nanotubes by nonlocal finite element method. *Eur Phys J Plus* 135(4):381
- Kandasamy R, Dimitri R, Tornabene F (2016) Numerical study on the free vibration and thermal buckling behavior of moderately thick functionally graded structures in thermal environments. *Compos Struct* 157:207–221
- Mantari J, Ore M (2015) Free vibration of single and sandwich laminated composite plates by using a simplified FSDT. *Compos Struct* 132:952–959
- Avcar M (2019) Free vibration of imperfect sigmoid and power law functionally graded beams. *Steel Compos Struct* 30(6):603–615
- Civalek Ö (2017) Free vibration of carbon nanotubes reinforced (CNTR) and functionally graded shells and plates based on FSDT via discrete singular convolution method. *Compos B Eng* 111:45–59
- Fakher M, Hosseini-Hashemi S (2020) Vibration of two-phase local/nonlocal Timoshenko nanobeams with an efficient shear-locking-free finite-element model and exact solution. *Eng Comput*. <https://doi.org/10.1007/s00366-020-01058-z>
- Ferreira A, Castro LM, Bertoluzza S (2009) A high order collocation method for the static and vibration analysis of composite plates using a first-order theory. *Compos Struct* 89(3):424–432
- Neves A, Ferreira A, Carrera E et al (2013) Free vibration analysis of functionally graded shells by a higher-order shear deformation theory and radial basis functions collocation, accounting for through-the-thickness deformations. *Eur J Mech-A/Solids* 37:24–34

22. Thai CH, Zenkour A, Wahab MA et al (2016) A simple four-unknown shear and normal deformations theory for functionally graded isotropic and sandwich plates based on isogeometric analysis. *Compos Struct* 139:77–95
23. Zenkour A (2005) A comprehensive analysis of functionally graded sandwich plates: part 2—buckling and free vibration. *Int J Solids Struct* 42(18–19):5243–5258
24. Zenkour AM (2013) Bending analysis of functionally graded sandwich plates using a simple four-unknown shear and normal deformations theory. *J Sandwich Struct Mater* 15(6):629–656
25. Mehar K, Kumar Panda S, Devarajan Y et al (2019) Numerical buckling analysis of graded CNT-reinforced composite sandwich shell structure under thermal loading. *Compos Struct* 216:406–414
26. Houari MSA, Tounsi A, Bég OA (2013) Thermoelastic bending analysis of functionally graded sandwich plates using a new higher order shear and normal deformation theory. *Int J Mech Sci* 76:102–111
27. Bourada M, Tounsi A, Houari MSA et al (2012) A new four-variable refined plate theory for thermal buckling analysis of functionally graded sandwich plates. *J Sandwich Struct Mater* 14(1):5–33
28. Ebrahimi F, Barati MR, Civalek Ö (2020) Application of Chebyshev-Ritz method for static stability and vibration analysis of nonlocal microstructure-dependent nanostructures. *Eng Comput* 36:953–964
29. Ebrahimi F, Farazmandnia N, Kokaba MR et al (2019) Vibration analysis of porous magneto-electro-elastically actuated carbon nanotube-reinforced composite sandwich plate based on a refined plate theory. *Eng Comput*. <https://doi.org/10.1007/s00366-019-00864-4>
30. Qaderi S, Ebrahimi F (2020) Vibration analysis of polymer composite plates reinforced with graphene platelets resting on two-parameter viscoelastic foundation. *Eng Comput*. <https://doi.org/10.1007/s00366-020-01066-z>
31. Zenkour A (2005) A comprehensive analysis of functionally graded sandwich plates: Part 1—Deflection and stresses. *Int J Solids Struct* 42(18–19):5224–5242
32. Hadji L, Atmane HA, Tounsi A et al (2011) Free vibration of functionally graded sandwich plates using four-variable refined plate theory. *Appl Math Mech* 32(7):925–942
33. Neves A, Ferreira A, Carrera E et al (2012) A quasi-3D sinusoidal shear deformation theory for the static and free vibration analysis of functionally graded plates. *Compos B Eng* 43(2):711–725
34. Neves A, Ferreira A, Carrera E et al (2012) A quasi-3D hyperbolic shear deformation theory for the static and free vibration analysis of functionally graded plates. *Compos Struct* 94(5):1814–1825
35. Neves A, Ferreira A, Carrera E et al (2013) Static, free vibration and buckling analysis of isotropic and sandwich functionally graded plates using a quasi-3D higher-order shear deformation theory and a meshless technique. *Compos B Eng* 44(1):657–674
36. Ye R, Zhao N, Yang D et al (2020) Bending and free vibration analysis of sandwich plates with functionally graded soft core, using the new refined higher-order analysis model. *J Sandw Struct Mater*. <https://doi.org/10.1177/1099636220909763>
37. Meziane MAA, Abdelaziz HH, Tounsi A (2014) An efficient and simple refined theory for buckling and free vibration of exponentially graded sandwich plates under various boundary conditions. *J Sandw Struct Mater* 16(3):293–318
38. Nguyen V-H, Nguyen T-K, Thai H-T et al (2014) A new inverse trigonometric shear deformation theory for isotropic and functionally graded sandwich plates. *Compos B Eng* 66:233–246
39. Bennoun M, Houari MSA, Tounsi A (2016) A novel five-variable refined plate theory for vibration analysis of functionally graded sandwich plates. *Mech Adv Mater Struct* 23(4):423–431
40. Meksi R, Benyoucef S, Mahmoudi A et al (2019) An analytical solution for bending, buckling and vibration responses of FGM sandwich plates. *J Sandw Struct Mater* 21(2):727–757
41. Sayyad AS, Ghugal YM (2019) A unified five-degree-of-freedom theory for the bending analysis of softcore and hardcore functionally graded sandwich beams and plates. *J Sandw Struct Mater*. <https://doi.org/10.1177/1099636219840980>
42. Belkhdja Y, Ouinas D, Zaoui FZ et al (2020) An exponential-trigonometric higher order shear deformation theory (HSDT) for bending, free vibration, and buckling analysis of functionally graded materials (FGMs) plates. *Adv Compos Lett* 29:0963693519875739
43. Saini R, Lal R (2020) Axisymmetric vibrations of temperature-dependent functionally graded moderately thick circular plates with two-dimensional material and temperature distribution. *Eng Comput*. <https://doi.org/10.1007/s00366-020-01056-1>
44. Sharma R, Jadon V, Singh B (2015) A review on the finite element methods for heat conduction in functionally graded materials. *J Inst Eng* 96(1):73–81
45. Chareonsuk J, Vessakosol P (2011) Numerical solutions for functionally graded solids under thermal and mechanical loads using a high-order control volume finite element method. *Appl Therm Eng* 31(2–3):213–227
46. Pandey S, Pradyumna S (2018) Analysis of functionally graded sandwich plates using a higher-order layerwise theory. *Compos B Eng* 153:325–336
47. Belarbi M-O, Tati A, Ounis H et al (2017) On the free vibration analysis of laminated composite and sandwich plates: a layerwise finite element formulation. *Latin Am J Solids Struct* 14(12):2265–2290
48. Das M, Barut A, Madenci E et al (2006) A triangular plate element for thermo-elastic analysis of sandwich panels with a functionally graded core. *Int J Numer Meth Eng* 68(9):940–966
49. Talha M, Singh B (2010) Static response and free vibration analysis of FGM plates using higher order shear deformation theory. *Appl Math Model* 34(12):3991–4011
50. Natarajan S, Manickam G (2012) Bending and vibration of functionally graded material sandwich plates using an accurate theory. *Finite Elem Anal Des* 57:32–42
51. Nguyen T-K, Nguyen V-H, Chau-Dinh T et al (2016) Static and vibration analysis of isotropic and functionally graded sandwich plates using an edge-based MITC3 finite elements. *Compos B Eng* 107:162–173
52. Gupta A, Talha M, Singh B (2016) Vibration characteristics of functionally graded material plate with various boundary constraints using higher order shear deformation theory. *Compos B Eng* 94:64–74
53. Kulikov G, Plotnikova S, Carrera E (2018) A robust, four-node, quadrilateral element for stress analysis of functionally graded plates through higher-order theories. *Mech Adv Mater Struct* 25(15–16):1383–1402
54. Carrera E (2003) Historical review of Zig-Zag theories for multilayered plates and shells. *Appl Mech Rev* 56(3):287–308
55. Li D (2020) Layerwise theories of laminated composite structures and their applications: a review. *Arch Comput Methods Eng*. <https://doi.org/10.1007/s11831-019-09392-2>
56. Raissi H, Shishehsaz M, Moradi S (2019) Stress distribution in a five-layer sandwich plate with FG face sheets using layerwise method. *Mech Adv Mater Struct* 26(14):1234–1244
57. Belarbi MO, Tati A (2015) A new C0 finite element model for the analysis of sandwich plates using combined theories. *Int J Struct Eng* 6(3):212–239
58. Belarbi M-O, Tati A, Ounis H et al (2016) Development of a 2D isoparametric finite element model based on the layerwise approach for the bending analysis of sandwich plates. *Struct Eng Mech* 57(3):473–506

59. Nikbakht S, Salami SJ, Shakeri M (2019) A 3D full layer-wise method for yield achievement in Functionally Graded Sandwich Plates with general boundary conditions. *Eur J Mech-A/Solids* 75:330–347
60. Carrera E (2002) Theories and finite elements for multilayered, anisotropic, composite plates and shells. *Arch Comput Methods Eng* 9(2):87–140
61. Pluciński P, Jaśkowiec J (2020) Three-dimensional analysis of laminated plates with functionally graded layers by two-dimensional numerical model. *Eng Trans* 68(1):21–45. <https://doi.org/10.24423/EngTrans.1063.20200102>
62. Iurlaro L, Gherlone M, Di Sciuva M (2014) Bending and free vibration analysis of functionally graded sandwich plates using the Refined Zigzag Theory. *J Sandw Struct Mater* 16(6):669–699
63. Belarbi MO, Tati A (2016) Bending analysis of composite sandwich plates with laminated face sheets: new finite element formulation. *J Solid Mech* 8(2):280–299
64. Reddy JN (1993) An evaluation of equivalent-single-layer and layerwise theories of composite laminates. *Compos Struct* 25(1–4):21–35
65. Liew K, Pan Z, Zhang L (2019) An overview of layerwise theories for composite laminates and structures: development, numerical implementation and application. *Compos Struct* 316:240–259
66. Liu M, Cheng Y, Liu J (2015) High-order free vibration analysis of sandwich plates with both functionally graded face sheets and functionally graded flexible core. *Compos B Eng* 72:97–107
67. Zenkour AM (2006) Generalized shear deformation theory for bending analysis of functionally graded plates. *Appl Math Model* 30(1):67–84
68. Reddy J (2000) Analysis of functionally graded plates. *Int J Numer Meth Eng* 47(1–3):663–684
69. Delale F, Erdogan F (1983) The crack problem for a nonhomogeneous plane. *J Appl Mech* 50:609–614
70. Nguyen TN, Thai CH, Nguyen-Xuan H (2016) A novel computational approach for functionally graded isotropic and sandwich plate structures based on a rotation-free meshfree method. *Thin-Walled Struct* 107:473–488
71. Gilhooley D, Batra R, Xiao J et al (2007) Analysis of thick functionally graded plates by using higher-order shear and normal deformable plate theory and MLPG method with radial basis functions. *Compos Struct* 80(4):539–552
72. Uymaz B, Aydogdu M (2007) Three-dimensional vibration analyses of functionally graded plates under various boundary conditions. *J Reinf Plast Compos* 26(18):1847–1863
73. Jin G, Su Z, Shi S et al (2014) Three-dimensional exact solution for the free vibration of arbitrarily thick functionally graded rectangular plates with general boundary conditions. *Compos Struct* 108:565–577
74. Xiang S, Kang G-W, Yang M-S et al (2013) Natural frequencies of sandwich plate with functionally graded face and homogeneous core. *Compos Struct* 96:226–231
75. Alibeigloo A, Alizadeh M (2015) Static and free vibration analyses of functionally graded sandwich plates using state space differential quadrature method. *Eur J Mech-A/Solids* 54:252–266

**Publisher's Note** Springer Nature remains neutral with regard to jurisdictional claims in published maps and institutional affiliations.